

Preprint IHEP-98-84  
hep-ph/0110152

# A New Scaling for Single-Spin Asymmetry in Meson and Baryon Hadroproduction

V.V.Abramov<sup>1</sup>

Experimental Physics Department,  
Institute for High Energy Physics, P.O. Box 35,  
Protvino, 142281 Moscow region, Russia

<sup>1</sup>E-mail: abramov\_v@mx.ihep.su

## Abstract

Experimental data on analyzing power for inclusive meson and baryon production in hadron-proton(polarized) collisions have been analyzed. It is found that the existing data can be described by a simple function of collision energy ( $\sqrt{s}$ ), transverse momentum ( $p_T$ ) and a new scaling variable  $x_A = E/E^{BEAM}$ . At beam energies above 40 GeV and  $p_T$  above 1 GeV/c the analyzing power is described by a function of  $x_A$  and  $p_T$  only ( $A_N = F(p_T)G(x_A)$ ) for both polarized proton fragmentation and central regions of proton-hadron collision. Comparison of data from Fermilab and new IHEP data measured using 40 GeV/c polarized proton beam was most decisive for the revelation of the above regularities. This new scaling law allows one to predict the analyzing powers for kinematic regions, not yet explored in experiments and constrains models of strong interactions. The new scaling law allows one also to use some reactions as polarimeters for experiments with a polarized beam.

*Keywords:* Inclusive Reaction; Polarization; Asymmetry; Spin; QCD  
*PACS:* 13.85.Ni; 13.88.+e; 12.38.Qk

Submitted to *Eur. Phys. J. C*

# 1 Introduction

In this paper we will study from empirical point of view the existing world data for one measured spin-dependent quantity (analyzing power) in collisions of unpolarized hadrons with polarized protons and antiprotons. The analyzing power ( $A_N$ ), which is often called single-spin asymmetry, should be distinguished from a raw asymmetry ( $A_{RAW}$ ), which is directly measured in experiments and depends on a beam (or target) polarization  $P_B$  ( $P_T$ ) and a dilution factor  $f$ . For polarized beam experiments  $A_{RAW} = A_N \cdot P_B$ , and for polarized target experiments  $A_{RAW} = A_N \cdot P_T/f$ .

Practically all existing data (with  $p \geq 6$  GeV/c) at intermediate and high energies are used for the analysis. Comparison of the Fermilab data [1], measured at 200 GeV/c with new 40 GeV/c IHEP polarized beam data [2] was an important step in the revelation of scaling features of the analyzing power.

The data measured with meson beams using polarized targets [3, 4, 5] are just briefly explored here. The important investigations in this field were done at the IHEP and other accelerators and merit probably a dedicated paper.

Recent measurements have shown that at high enough energies the analyzing power for inclusive production of hadrons in reactions

$$h_1^\uparrow h_2 \rightarrow h_3 + X$$

where  $h_1$ ,  $h_2$  and  $h_3$  are hadrons, is large and described by a simple function of kinematic variables and shows an approximate scaling in  $x_F = 2p_Z^*/\sqrt{s}$  for fragmentation region of vertically polarized protons and a scaling in  $x_T = 2p_T/\sqrt{s}$  for central region [1, 2, 6]–[9]. It is larger in the fragmentation region of polarized protons (antiprotons) than in the central region. Some authors have assumed, that for the analyzing powers a radial scaling takes place ( $x_R = 2p^*/\sqrt{s}$ ) [9, 10]. However, as will be shown below, this assumption has not been confirmed. The purpose of this study is to find a suitable scaling variable, that allows one to describe in a unified way the dependence of analyzing powers on kinematic variables in a wide range of beam energies, transverse momenta, and angles of particle production.

A thorough study of the existing data has shown that the analyzing power for the inclusive  $\pi^+$ -meson production in  $p^\uparrow p$  collisions has the following fea-

tures [1, 2, 9]:

- a) the scaling and linear dependence on  $x_F$  or  $x_T$  in the region of polarized proton fragmentation or in the central region, respectively;
- b) the analyzing power maximum in the fragmentation region (near  $x_F=1$ ) is approximately two times higher than it is in the central region (near  $x_T=1$ );
- c) the analyzing power changes its sign (or is zero) in the polarized proton fragmentation region at  $x_F$  near 0.18, whereas in the central region it takes place at  $x_T$  near 0.37, which is approximately two times higher;
- d) the analyzing power grows with  $p_T$  rise at fixed  $x_F$ , has a plateau above 1 GeV/c, and probably decreases when  $p_T$  gets much higher 1 GeV/c;
- e) the analyzing power is zero at  $p_T = 0$  due to the azimuthal symmetry of cross section.

Feature (d) has not too much experimental conformation yet, but below it is assumed to be valid.

The features (a), (b) and (c) are well explained if we assume that at high enough energy and  $p_T$  the analyzing power is described by a function of  $p_T$  and a new scaling variable ( $x_A$ ):

$$A_N = F(p_T)G(x_A). \quad (1)$$

The scaling variable  $x_A$  is defined as

$$x_A = E/E^{BEAM}, \quad (2)$$

where  $E$  and  $E^{BEAM}$  are energies of the detected particle ( $\pi^+$ ) and the beam particle (proton), respectively, in the laboratory frame, and a polarized beam particle collides with a target at rest. This occurs because in the fragmentation region  $x_A$  is close to  $x_F$  and its maximum is equal to 1.0, whereas in the central region  $x_A$  is close to  $0.5 \cdot x_T$  and its maximum is equal to 0.5, when beam energy is divided between two high  $x_T$  jets (particles). In case of experiments with a polarized target [3, 4, 5, 10, 11, 14],  $x_A$  is calculated in anti-laboratory frame, where a beam particle is again a transversely polarized

proton. Eq. (2) takes the form  $x_A = p_{h_3} \cdot p_{h_2} / p_{h_1} \cdot p_{h_2}$  when it is expressed in the Lorentz-invariant way.

The eq. (1) means not only a scaling law for  $A_N$ , but in addition a factorization of  $p_T$  and  $x_A$  dependences. This factorization simplifies the analysis and is in agreement with the existing data, as will be shown below.

We expect that most (but not all) of the specified above analyzing power features (a – e) are valid not only for  $\pi^+$  production, but also for other pseudoscalar mesons ( $\pi^-$ ,  $\pi^0$ ,  $K^\pm$ ,  $K_S$ ,  $\eta$ ), as well as for some baryons (protons, antiproton, hyperons), though the experimental information for some of them is very limited. In particular, feature (e) is valid for any considered reaction, since the normal vector to the scattering plane is undefined when  $p_T = 0$ , and no left-right asymmetry exists. Of course, at  $x_A = 0$  analyzing power is also zero, but this is not an independent feature, since in this case  $p_T = 0$ . Feature (e) means that  $F(0) = 0$ , but it does not mean that  $G(0) = 0$ . In particular,  $A_N$  as a function of  $x_A$  at fixed value of  $p_T \neq 0$  will not tend to zero when  $x_A$  approaches zero. On the other hand if we consider  $A_N$  measurements at fixed laboratory angle, as often happens,  $p_T \propto x_A$  and  $A_N$  tends to zero when  $x_A$  approaches zero.

There are several alternative variables which are numerically close to the  $x_A$  variable, given by eq. (2). In particular,

$$x_A' = (x_F + x_R)/2, \quad (3)$$

$$x_A'' = (E + P_Z)/(E^{BEAM} + P_Z^{BEAM}), \quad (4)$$

$$x_A''' = P/P^{BEAM}, \quad (5)$$

where  $P$  and  $P^{BEAM}$  are momenta of the detected particle and beam particle, respectively, in the laboratory frame. All of them are very close to each other at high energies and the choice of the best scaling variable requires additional and very accurate measurements of the analyzing power and kinematic variables. Eq. (3) gives a very transparent explanation of the  $x_F$ -scaling in the fragmentation region and the  $x_T$ -scaling in the central region.

The proposed scaling may be applied to the inclusive production of hadrons in the collisions of polarized protons with light nuclei. Analyzing powers measured in reactions  $p^\uparrow p \rightarrow h + X$  and  $p^\uparrow d \rightarrow h + X$ , where  $h$  is a charged hadron ( $\pi^\pm$ ,  $K^\pm$ , or  $p$ ) agree within the errors [12]. Reactions with pion beam and polarized proton or deuteron targets also give analyzing power for  $\pi^0$  production independent of the target within the errors [5].

Similar methods of different empirical scalings were used for the description of features of other reactions or observables. An example may be a description of the analyzing power in  $p^\uparrow C$  collisions with one outgoing charged particle. This reaction was often used for the polarimetry purposes (see e.g. [13] and references therein). In this and other similar cases an empirical description of one of observables seem to be a correct way to show common characteristics as well as possible hidden features of strong interaction.

A thorough study of the available experimental data on the analyzing powers is presented in the subsequent sections.

## 2 Analyzing power for $p^\uparrow p \rightarrow \pi^+ + X$ reaction

For the study of scaling features of the analyzing power all the available experimental data are presented in the frame in which a polarized proton is a projectile with spin directed upward and the target is at rest. The analyzing power is considered positive when more hadrons are produced to the left in the horizontal plane looking in the direction of the incident beam. Thus, the original sign of the analyzing power for experiments [11, 14] has been changed to the opposite one, in agreement with the definition given above. Kinematic variables for the experiments which used polarized target have been transformed into the anti-laboratory frame. Unfortunately, not all authors in their publications presented a complete set of variables ( $\sqrt{s}$ ,  $p_T$ ,  $x_F$ ) for each point. For some experiments only limits on these variables are given that makes transformation to other variables biased and limits accuracy of the  $x_A$ -scaling check. Additional error ( $\epsilon = \pm 0.025$ ) is added in quadrature to all errors of  $A_N$ -values to take into account possible variable bias and systematic errors during the fitting procedure below for  $\pi^+$ -meson production and other reactions if not stated otherwise.

The analyzing power of  $\pi^+$  production in  $p^\uparrow p$  collisions [1, 2, 9, 14] is shown in Figs. 1, 2 and 3 as a function of  $p_T$ ,  $x_R$ , and  $x_A$ , respectively. The highest  $p_T$  ( $\sim 3.5$  GeV/c) is reached in [2], and the highest energy ( $\sqrt{s} = 19.43$  GeV) in [1]. As is seen in Figs. 1 and 2, there is no scaling behaviour of the analyzing power as a function of  $p_T$  or  $x_R$ . Experiments, performed in forward, central and backward regions have an analyzing power, decreasing from the forward to backward region, with the central region in the middle. In Fig. 3 the analyzing power, as a function of  $x_A$ , shows approximate scaling

behaviour for all three regions, mentioned above. Only the subset of data [1] with  $p_T < 0.7$  GeV/c is below general trend, in agreement with the feature (d) above. The analyzing power dependence on  $x_A$  is close to a linear one in the consent with the feature (a) above. A simple expression, which takes into account all the features (a–e) and low energy corrections can be used to fit the data shown in Fig. 3:

$$A_{N1} = F(p_T) \cdot \begin{cases} c \cdot \sin(\omega(x_A - x_0)) + a_6/s, & \text{if } x_A \geq a_4; \\ c \cdot \sin(\omega((a_4 - x_0) + a_5(x_A - a_4))) + a_6/s, & \text{otherwise;} \end{cases} \quad (6)$$

where  $x_0$  is a constant. The perturbative QCD predicts the vanishing of the analyzing power at high  $p_T$  [15, 16]. The same asymptotic has function  $F(p_T)$ , which takes into account the above mentioned features (d) and (e)

$$F(p_T) = 2p_T m / (m^2 + p_T^2), \quad (7)$$

where  $p_T$  is measured in GeV/c and  $c, x_0, m, a_4 - a_6$  are free fit parameters. The exact shape of  $F(p_T)$  should be measured in future experiments. Parameters  $a_4, a_5$  and  $a_6$  are equal to zero, and  $\omega = 1$  for  $\pi^+$ -meson production. They are introduced for other reactions, considered below, to take into account possible nonlinearity and non-asymptotic contribution to the analyzing power at low energy. So, for  $\pi^+$  at high enough energy we have  $G(x_A) = c \cdot \sin(\omega(x_A - x_0))$ .

The point  $x_A = x_0$  may be interpreted as a point where the relative phase of two helicity amplitudes (spin-flip and spin-nonflip) passes through zero and, perhaps, changes its sign, as was suggested in [5]. This problem will be discussed in section 9. From experimental point of view the zero-crossing point of the analyzing power was observed not only in the reaction of  $\pi^0$  production by  $\pi^-$  beam [3, 4, 5], but similar indications were observed in some reactions of meson and baryon production by polarized proton beam [1, 2, 7, 9, 12, 17]. Experimental study of zero-crossing point is difficult because of small value of  $A_N$  and low setup efficiency near that point. The existence of zero-crossing point (with possible change of  $A_N$  sign near it) may be critical for many theoretical models.

Along with the experiments presented in Figs. 1–3, there is an experiment with very thorough measurements of the analyzing power at 11.75 GeV/c [12]. The measurements have been performed for a set of fixed secondary momenta, corresponding to fixed  $x_A$  values, and for each  $x_A$  as a function

of the production angle or  $p_T$ . The data are presented in Figs. 4 and 5, as a function of  $x_A$  and  $p_T$ , respectively. As is seen from Figs. 4 and 5, only the points corresponding to the highest available  $p_T$ , which are about 1 GeV/c, are close to the scaling function (6) and to the experimental points shown in Fig. 3 for higher energies. Dependence of  $A_N$  on  $p_T$  is very different from the corresponding behaviour at higher energies, shown in Fig. 1. To understand this difference of data [12] from the rest of the data, we have to assume that at 11.75 GeV/c ( $\sqrt{s} = 4.898$  GeV) and low  $p_T$  there exists an additional contribution to the analyzing power, which is approximated by the expression

$$A_{N0} = F_0(p_T) \left( b_1 \tanh(b_2(p_T - b_7)) \sin(b_8 x_A^{b_4}) + b_5 + b_6 x_A \right), \quad (8)$$

where function  $F_0(p_T)$  suppresses the analyzing power at low  $p_T$

$$F_0(p_T) = 2p_T^2 / (b_3^2 + p_T^2), \quad (9)$$

and  $b_1 - b_8$  are free parameters.

Fit of a combined data set, which includes the data, presented in Figs. 3 and 4, requires additional assumption that the  $A_{N0}$  contribution decreases with energy, and the complete analyzing power is

$$A_N = A_{N1} + A_{N0} \cdot (4.898/\sqrt{s})^{b_9}, \quad (10)$$

where  $b_9$  is a free parameter.

The results of the combined data set fit are presented in Figs. 3 and 4 (corresponding curves) and in Table 1 (fit parameters). Two subsets of the combined data are shown in the separate figures to give a clearer representation of 117 data points. Parameter  $\omega$  was fixed since the data show a linear dependence on  $x_A$  and the experimental accuracy is not sufficient to get  $c$  and  $\omega$  values separately. In all the fits below it is assumed that  $\omega = 1$ , unless otherwise specified. The agreement between the fitting curves and the data is rather good. The analysis has shown that the contribution of  $A_{N0}$  term to (10) is small ( $\leq 0.08$ ) for the experiments presented in Fig. 3. On the other hand, the term  $A_{N1}$  is significant ( $\leq 0.3$ ) for a kinematic region of the experiment [12], presented in Figs. 4 and 5.

The ratio of the experimental analyzing power and  $F(p_T)$ , which is expected to be a function of  $x_A$  only, with a possible small dependence on  $\sqrt{s}$ ,

Table 1: Fit parameters of eqs. (6)–(10) for  $\pi^+$ -mesons.

$c$	$x_0$	$m$	$a_6$
$0.69 \pm 0.08$	$0.170 \pm 0.046$	$2.0 \pm 0.4$	$0.00$
$\omega$	$b_1$	$b_2$	$b_3$
$1.00$	$0.148 \pm 0.029$	$8.6 \pm 2.3$	$0.35 \pm 0.07$
$b_4$	$b_5$	$b_6$	$b_7$
$4.8 \pm 1.0$	$0.004 \pm 0.015$	$-0.148 \pm 0.041$	$0.646 \pm 0.016$
$b_8$	$b_9$	N points	$\chi^2$
$5.6 \pm 2.6$	$2.0 \pm 1.9$	117	114.4

is shown in Fig. 6. The data from [12] are presented in Fig. 6 by two subsets, corresponding to  $0.8 \leq p_T \leq 0.9$  GeV/c and  $0.9 \leq p_T \leq 1.2$  GeV/c, respectively. All the experimental points in Fig. 6 are consistent with the simple function of  $x_A$

$$A_N/F(p_T) = c \cdot \sin(\omega(x_A - x_0)), \quad (11)$$

that confirms scaling behaviour and factorization of  $p_T$  and  $x_A$  dependencies, assumed in (1) and (6) at high  $p_T$  and high beam energy.

Recently, when this paper was already prepared for publication, new 21.6 GeV/c data for  $\pi^+$ ,  $\pi^-$  and proton production analyzing powers in  $p^\uparrow C$  collisions from the BNL E925 experiment have been measured [18], which confirm the  $A_N$  behaviour, predicted by eqs. (6-10). In particular, the value of  $x_A$ , where  $A_N$  approaches to zero, is much higher due to non-asymptotic contribution (8) in low  $p_T \leq 0.7$  GeV/c region. Corresponding points are shown in Figs. 3 and 6 along with predictions from eqs. (6-10). The last four points with  $p_T \geq 0.7$  GeV/c are compatible with general scaling behaviour of other data shown in Fig. 6. It has to be noted that only statistical errors are shown for data [18]. The overall statistical and systematic error in the beam polarization gives a relative scale uncertainty of 24% for  $A_N$ , the same for all three reactions of interest for all  $x_F$  and  $p_T$ . Due to this scale uncertainty

and the usage of different target (carbon) these data are not included in the overall fit and are shown for the purpose of comparison only.

The results of the fit (10) show that the data sample [12] can be compatible with the rest of the data assuming that the additional contribution (8) is significant only at low beam energy and  $p_T$ . The physical nature of this contribution, which is negative at  $p_T$  near 0.4 GeV/c even at high  $x_A$ , is not completely clear. It could be a resonance contribution [15, 19], or something else. The authors of [12] have assumed that the observed analyzing power is explained by the baryon exchange in  $u$ -channel.

The existing experimental data at higher energies, presented in Fig. 3, are not very sensitive to the contribution (8), which is prominent at 11.75 GeV/c. A detailed experimental study of region  $p_T \leq 1$  GeV/c at higher energies and different production angles could help to understand its nature.

Fit parameters of eq. (6) for different definitions of scaling variable (2) – (5) are presented in Table 2. Only parameters  $c, x_0, m$  are free here. All other parameters are the same as in Table 1. The difference in  $\chi^2$  is not very significant, with a weak preference for eqs. (2), (4) and (5) variables.

Table 2: Fit parameters of eq. (6) for  $\pi^+$ -mesons. Different definitions of the scaling variable  $x_A$  are used for comparison (eqs. (2)–(5)).

eq.	$c$	$x_0$	$m$	$\chi^2$
(2)	$0.69 \pm 0.08$	$0.170 \pm 0.047$	$2.0 \pm 0.4$	114.4
(3)	$0.74 \pm 0.07$	$0.166 \pm 0.013$	$2.2 \pm 0.3$	120.4
(4)	$0.69 \pm 0.07$	$0.167 \pm 0.013$	$2.1 \pm 0.3$	114.6
(5)	$0.68 \pm 0.06$	$0.170 \pm 0.013$	$2.0 \pm 0.2$	114.2

The error ( $\epsilon = \pm 0.025$ ), added in quadrature to the error of  $A_N$  at each data point during the fitting procedure, has not changed the fit parameters significantly, but has reduced  $\chi^2$  by about a factor of two up to a level of about unity per degree of freedom. Errors, shown in figures, representing experimental data, also include this additional error.

### 3 Analyzing power for $p^\uparrow p \rightarrow \pi^- + X$ reaction

The analyzing power for  $\pi^-$ -meson production by polarized protons [1, 2, 9, 14] is shown in Fig. 7 as a function of  $x_A$ . As with  $\pi^+$ -mesons, we observe an approximate scaling in the dependence of  $A_N$  vs  $x_A$ . Selection of the data with  $p_T \geq 0.8$  GeV/c and  $E^{BEAM} \geq 40$  GeV leads to a good agreement between two experiments [1, 2] which implies their scaling behaviour.

The new 21.6 GeV/c data for  $\pi^-$  production analyzing power in  $p^\uparrow C$  collisions from the BNL E925 experiment [18] are also shown in Fig. 7 along with predictions from eqs. (6-10). The last three points with  $p_T \geq 0.8$  GeV/c are compatible with general scaling behaviour observed at higher energies [1, 2]. Low  $p_T \leq 0.8$  GeV/c points deviate from the scaling law due to a non-asymptotic contribution (8). This is also a reason why  $A_N$  cross zero level at much higher value of  $x_A \approx 0.6$ . Only statistical errors are shown for data [18], while overall relative scale uncertainty for  $A_N$  is 24% .

Experiment [12] reveals quite different  $x_A$  and  $p_T$ -dependencies at 11.75 GeV/c, in Figs. 8 and 9, respectively. As with  $\pi^+$ , the greatest deviation from the scaling behaviour occurs at low  $p_T$ . At  $p_T = 0.15$  GeV/c the analyzing power is very large and positive in contrast to the large energy behaviour, where it is negative. One of possible origins of this low energy analysing power is probably the same as that discussed above for  $\pi^+$ -mesons, and its approximation is given by eqs. (6) – (10). The difference is that parameters  $a_4$  and  $a_6$  are now not equal to zero, while  $a_5 = 0$ . The non-linear dependence of  $A_N$  vs  $x_A$  is taken into account by setting  $a_4 > 0$  in eq. (6). Fit parameters of the combined data sample, shown in Figs. 7 and 8, are presented in Table 3. Some of the parameters could not be well determined from the existing data and were fixed ( $m = 4.8$ ,  $\omega = 1$ ) during the fitting procedure. The role of energy-dependent term ( $a_6/s$ ) is more significant for  $\pi^-$ , than for  $\pi^+$  mesons. Possible explanation can be related to resonance contribution [19]. The analyzing power in low  $x_A \leq 0.3$  region is close to zero in agreement with the expected large gluon contribution [15].

### 4 Analyzing power for $p^\uparrow p \rightarrow p + X$ reaction

The analyzing power for proton production has been measured at 6 different beam energies, from 6 up to 40 GeV [2, 9, 12, 14, 20]. It is shown in Fig. 10

Table 3: Fit parameters of eqs. (6)–(10) for  $\pi^-$ -mesons.

$c$	$x_0$	$m$	$a_4$
$-0.96 \pm 0.20$	$0.185 \pm 0.075$	4.80	$0.303 \pm 0.045$
$a_6$	$b_1$	$b_2$	$b_3$
$3.8 \pm 1.8$	$-0.345 \pm 0.089$	$8.0 \pm 2.8$	$0.115 \pm 0.024$
$b_4$	$b_5$	$b_6$	$b_7$
$3.1 \pm 0.5$	$-0.047 \pm 0.018$	$0.256 \pm 0.052$	$0.344 \pm 0.028$
$b_8$	$b_9$	N points	$\chi^2$
$1.12 \pm 0.27$	$0.76 \pm 0.39$	84	89.5

as a function of  $x_A$ . The absolute value of  $A_N$  is small ( $\leq 0.1$ ) and with the existing accuracy  $A_N$  is compatible with the approximate  $x_A$ -scaling, especially, when taking into account possible systematic errors of the order of 0.02. Nevertheless, the data fitting function (eq. (6)) is modified to give a better approximation. In particular, the fit approximates the data better if a fitting function is not suppressed at high  $p_T$ , as is the case with eq. (7). Non-asymptotic contribution to  $A_N$  at low energies is more significant for protons than for  $\pi^-$ -mesons and was approximated by  $a_6/s^{0.5}$  term. Eqs. (12) and (13) are used to fit the proton production analyzing power

$$A_N = F_P(p_T)(c \cdot \sin(\omega(x_A - x_0)) + a_6/s^{0.5}), \quad (12)$$

where

$$F_P(p_T) = 1 - \exp(-p_T/m). \quad (13)$$

Function  $F_P(p_T)$  makes valid feature (e) of zero  $A_N$  at  $p_T = 0$ . An extra error  $\epsilon = \pm 0.015$  is added to the error of  $A_N$  at each data point. The comparison of fit parameters for different definitions of  $x_A$ , given by eqs. (2)–(5), is shown in Table 4. The best  $\chi^2$  is reached if  $x_A$  is given by eq. (4). The analyzing power slightly rises with  $x_A$  increase and changes its sign near  $x_A = 0.5$  at beam energies around 10 GeV. Additional measurements of  $A_N$  for protons

Table 4: Fit parameters of eqs. (12–13) for the protons and different definitions of the scaling variable  $x_A$ , eqs. (2) –(6). Parameters  $a_4 - a_5$  are set equal to zero and  $\omega = 1$  during the fit.

eq.	$c$	$x_0$	$m$	$a_6$	$\chi^2$ / points
(2)	0.116 $\pm$ 0.011	0.81 $\pm$ 0.15	0.184 $\pm$ 0.006	0.216 $\pm$ 0.080	120.9/ 150
(3)	0.117 $\pm$ 0.012	0.90 $\pm$ 0.13	0.186 $\pm$ 0.007	0.316 $\pm$ 0.078	125.6/ 150
(4)	0.117 $\pm$ 0.011	0.82 $\pm$ 0.14	0.187 $\pm$ 0.006	0.230 $\pm$ 0.080	118.6/ 150
(5)	0.117 $\pm$ 0.011	0.83 $\pm$ 0.14	0.187 $\pm$ 0.006	0.236 $\pm$ 0.079	119.4/ 150

at higher energies in the fragmentation region of polarized protons could help to clarify a possible energy dependence of the analyzing power.

The new 21.6 GeV/c data for proton production analyzing power in  $p^\uparrow C$  collisions from the BNL E925 experiment [18] are also shown in Fig. 10 along with predictions from eqs. (12–13). The data are compatible with general trend of  $A_N$  rise with increase of  $x_A$ . Only statistical errors are shown for data [18], while overall relative scale uncertainty for  $A_N$  is 24%.

## 5 Analyzing powers for $\pi^0$ , $K^+$ , $K^-$ and $\bar{p}$ production by polarized protons

The analyzing power for  $\pi^0$ -meson production in  $p^\uparrow p$  collisions has been measured at 24, 185 and 200 GeV/c [7, 8, 11, 21, 22]. The data are shown in Fig. 11 as a function of  $x_A$ . They are compatible with a simple dependence given by eq. (6) with  $a_4 = 0$  and  $a_6 = 0$ . The fit parameters are shown in Table 5. The data [11] were measured using a polarized target, where the dilution factor plays an important role, reaches large values (and also errors) and may be badly determined. A very large analyzing power observed in a few points with largest  $p_T$  at 24 GeV/c [11] probably results from the above problem of dilution factor measurement.

Assumption of the  $x_A$ -scaling allows one to explain the enigma of the

E704 data [7], which have not shown any significant analyzing power, though experiment has reached high  $p_T$  values up to 4.5 GeV/c. This is because the corresponding values of  $x_A$  are near  $x_0 = 0.111$ , where  $A_N$  as a function of  $x_A$  is close to zero. Both, the high  $p_T$  [7], and the high  $x_F$  [8] data are in good agreement if plotted vs  $x_A$ .

The analyzing power for  $K^+$ -meson production in  $p^\uparrow p$ -collisions has been measured in two experiments [2, 12] at 40 and 11.75 GeV/c, respectively. It is shown in Fig. 12 as a function of  $x_A$ . The  $A_N$  dependence on kinematic variables was approximated by eq. (6) with  $a_4 = 0$  and  $a_6 = 0$ , because statistical accuracy of the data is limited. The fit parameters are presented in Table 5. The experimental data are compatible with the  $x_A$ -scaling (see eq. (6)).

The analyzing power for  $K^-$ -meson production has been measured at 40 and 11.75 GeV/c [2, 12]. It was fitted by eq. (6) with  $a_6$ , as a free parameter and  $a_4 = 0$ . The energy dependent term  $a_6/s$  significantly improves the fit for  $K^-$ , in contrast to the  $K^+$  case. The parameters of the fit are shown in Table 5. The ratio  $A_N/F(p_T)$  is shown in Fig. 13 vs  $x_A$ , where the shift of data points due to  $a_6/s$  term is clearly seen. The parameter  $m$  for  $K^-$ -meson, which has no valence quarks common for colliding protons, is much smaller than in the case with  $K^+$ -meson and is close to the estimation of Ref. [15]. Contrary to  $\pi^\pm$ -mesons,  $K^\pm$ -mesons do not show any unusual behaviour at 11.75 GeV/c which requires an additional contribution to the analyzing power similar to that given by eq. (8).

The analyzing power for antiprotons has been measured only at 40 GeV/c at one fixed laboratory angle [2]. Therefore, it is impossible to determine parameter  $m$ , which was fixed at 1 GeV/c during the fit of the data by eq. (6). The fit parameters are presented in Table 5 and  $A_N$  vs  $x_A$  is shown in Fig. 14. Additional measurements are required for  $K^+$ ,  $K^-$ -mesons, and antiprotons at different energies and production angles to check the  $x_A$ -scaling and determine the parameters of eq. (6).

Table 5: Fit parameters of eq. (6) for the  $\pi^0$ ,  $K^+$ ,  $K^-$ -mesons and  $\bar{p}$ . Parameters  $a_4 - a_5$  are set equal to zero and  $\omega = 1$  during the fit, with  $\epsilon = \pm 0.015$  for  $\pi^0$  and  $\epsilon = \pm 0.010$  for  $K^+$ ,  $K^-$ ,  $\bar{p}$ .

$h_3$	$c$	$x_0$	$m$	$a_6$	$\chi^2$ / points
$\pi^0$	$0.24 \pm 0.04$	$0.111 \pm 0.019$	$1.40 \pm 0.49$	0	50.5 / 54
$K^+$	$0.37 \pm 0.08$	$0.183 \pm 0.045$	$1.15 \pm 0.34$	0	65.8 / 67
$K^-$	$1.88 \pm 0.34$	$0.086 \pm 0.054$	$0.25 \pm 0.07$	$-13.5 \pm 4.2$	24.2 / 28
$\bar{p}$	$0.6 \pm 1.0$	$0.16 \pm 0.12$	1.00	0	15.6 / 11

## 6 Analyzing powers for $\Lambda$ , $K_S^0$ , $\eta$ production by polarized protons

The analyzing power for the  $\Lambda$ -hyperon production has been measured at 13.3, 18.5 and 200 GeV/c [23, 24]. It is shown as a function of  $x_A$  in Fig. 15 along with fitting curves (eq. (6)). Data [23] were obtained on a Be target, and data [24] on a proton target. The fit parameters for different  $x_A$  definitions are presented in Table 6. The best  $\chi^2$  is attained with  $x_A$  defined by eq. (3). As is seen from Fig. 15,  $A_N$  can be described at different energies by the same function of the scaling variable  $x_A$  at the present level of experimental errors. The analyzing power is close to zero for the region  $0.2 \leq x_A \leq 0.6$  and is negative for the  $x_A$  above 0.6.

Measurements of  $A_N$  for the  $K_S^0$ -mesons have been performed at 13.3 and 18.5 GeV in the central region only [23, 25], both on a Be target. In Fig. 16  $A_N$  is shown as a function of  $x_A$  along with a fitting curve given by eq. (6). The fit parameters are presented in Table 7. The data are compatible with the  $x_A$ -scaling, but additional measurements are desirable to check it at different energies and in the fragmentation region.

The analyzing power for the  $\eta$ -meson production in  $p^\uparrow p$  collisions has been measured at 200 GeV/c [17]. It is shown in Fig. 17 along with the

Table 6: Fit parameters of eq. (6) for the  $\Lambda$  and different definitions of scaling variable  $x_A$ , eqs. (2) –(5), with  $\epsilon = \pm 0.015$  and  $\omega = 1$ .

eq.	$c$	$x_0$	$m$	$a_4$	$a_5$	$\chi^2$ / points
(2)	$-0.52 \pm 0.15$	$0.557 \pm 0.036$	$0.66 \pm 0.36$	$0.563 \pm 0.035$	$-0.111 \pm 0.096$	39.4 / 49
(3)	$-0.72 \pm 0.38$	$0.539 \pm 0.021$	$1.6 \pm 1.3$	$0.527 \pm 0.024$	$-0.158 \pm 0.073$	24.3 / 49
(4)	$-0.54 \pm 0.15$	$0.560 \pm 0.034$	$0.69 \pm 0.37$	$0.564 \pm 0.033$	$-0.109 \pm 0.091$	38.3 / 49
(5)	$-0.53 \pm 0.15$	$0.559 \pm 0.034$	$0.68 \pm 0.37$	$0.564 \pm 0.034$	$-0.109 \pm 0.091$	38.5 / 49

Table 7: Fit parameters of eq. (6) for the  $K_S^0$  and  $\eta$ -mesons, with  $\epsilon = \pm 0.015$  and  $\omega = 1$ .

$h_3$	$c$	$x_0$	$m$	$\chi^2$ / points
$K_S^0$	$-0.143 \pm 0.095$	$-0.49 \pm 0.50$	$0.79 \pm 0.49$	4.4 / 16
$\eta$	$1.00 \pm 0.36$	$0.323 \pm 0.048$	1.00	0.0 / 4

fitting curve, eq. (6). The fit parameters are shown in Table 7. Since the measurement has been performed at a fixed angle, parameter  $m$  was fixed during the fit.

## 7 Analyzing powers for the $\pi^\pm$ , $\pi^0$ and $\eta$ production in $\bar{p}^\uparrow p$ collisions

The analyzing power for the  $\pi^\pm$ -meson production in the fragmentation region of polarized antiprotons has been measured at 200 GeV/c [6]. It is shown in Figs. 18 and 19, as a function of  $x_A$ , for the  $\pi^+$  and  $\pi^-$ , respectively. The fit parameters are presented in Table 8. Parameter  $m$  has been fixed due to

limited statistics.

Table 8: Fit parameters of eq. (6) for the  $\pi^\pm$ ,  $\pi^0$ , and  $\eta$ -meson production in  $\bar{p}p$ -collisions, with  $\epsilon = \pm 0.015$ .

$h_3$	$c$	$x_0$	$m$	$\omega$	$\chi^2$ / points
$\pi^+$	$-0.32 \pm 0.20$	$0.344 \pm 0.020$	1.0	$2.8 \pm 2.1$	10.4 / 10
$\pi^-$	$0.23 \pm 0.10$	$0.309 \pm 0.035$	1.0	$2.8 \pm 1.8$	10.1 / 10
$\pi^0$	$0.15 \pm 0.07$	$0.050 \pm 0.061$	$1.5 \pm 1.3$	1.0	21.1 / 34
$\eta$	$-1.1 \pm 0.9$	$0.468 \pm 0.075$	1.0	1.0	0.9 / 3

Measurements of  $A_N$  for the  $\pi^0$ -meson production in  $\bar{p}^\uparrow p$ -collisions has been performed at 200 GeV/c in the central region [7] and the fragmentation region [22] of polarized antiprotons. The data are shown as a function of  $x_A$  along with the fitting curve (eq. (6)) in Fig. 20. The fit parameters are shown in Table 8. As in the case of polarized proton beam, high  $p_T$  data do not show any significant analyzing power, in agreement with the predictions of  $x_A$ -scaling.

The analyzing power for the  $\eta$ -meson production has been measured just in a few points at 200 GeV/c [17]. The fit parameters are shown in Table 8.

It is easy to notice that  $x_0$ -parameter for the  $\pi^\pm$  and  $\eta$ -meson production by polarized antiprotons is by about 0.15 larger as compared to the case of polarized proton beam.

## 8 Asymmetries for the $\pi^0$ and $\eta$ production in $\pi^- p^\uparrow$ collisions

Asymmetry measurements for the  $\pi^0$  and  $\eta$ -meson production have been carried out at 40 GeV/c in the central region [3] and in the fragmentation region of  $\pi^-$ -meson [4]. The data for the  $\pi^0$ -mesons are shown in Fig. 21 along with the fitting curve (eq. (6)). The dashed curve shows the prediction of eq. (6) for region  $0.03 \leq x_A \leq 0.1$  and  $p_T = 1$  GeV/c, where no data exist

and a local minimum of  $A_N$  is expected from the fit. The dash-dot curve shows the prediction for region  $p_T = 2$  GeV/c and  $x_A \geq 0.3$ , where a local maximum of  $A_N$  is expected near  $x_A = 0.3$ , and a local minimum is expected near  $x_A = 0.5$ . The use of  $\sin(\omega(x_A - x_0))$  with large  $\omega$  value in eq. (6) allows one to satisfy the constrain  $|A_N| \leq 1$ . The fit parameters are shown in Table 9. The values of  $\omega$  shown in Table 9 are the minimal ones which satisfy the constrain  $|A_N| \leq 1$ .

Table 9: Fit parameters of eq. (6) for the  $\pi^0$  and  $\eta$ -meson production in  $\pi^-p$ -collisions, with  $\epsilon = 0.015$ .

$h_3$	$c$	$x_0$	$m$	$a_4$	$a_5$	$\omega$	$\chi^2$ / points
$\pi^0$	$1.0 \pm 0.4$	$0.131 \pm 0.008$	$0.3 \pm 1.3$	$0.078 \pm 0.062$	$-0.8 \pm 1.7$	12.0	15.2 / 20
$\eta$	$1.0 \pm 0.5$	$0.154 \pm 0.016$	1.0	0.0	0.0	12.5	0.2 / 3

The asymmetry vs  $x_A$  for the  $\eta$ -meson production is shown in Fig. 22. Since only a few experimental points have been measured, some of the parameters of eq. (6) were fixed (see Table 9). Predictions for region  $x_A \leq 0.15$  and  $p_T = 1$  GeV/c are shown by the dashed curve, and predictions for region  $x_A \geq 0.3$  and  $p_T = 2$  GeV/c are shown in Fig. 22 by the dash-dot curve. As in the case of  $\pi^0$  production, a local maximum of  $A_N$  is expected (near  $x_A = 0.3$ ). Also a local minimum of  $A_N$  is expected near  $x_A = 0.5$ . For both  $\pi^0$  and  $\eta$ -meson production by  $\pi^-$  beam, the dependence on  $x_A$  looks very similar having a fast rise in the range  $0.15 \leq x_A \leq 0.3$ . This behaviour is very different from the  $x_A$ -dependence in  $p^\uparrow p$ -collisions, where the rise of  $A_N$  with  $x_A$  is not so dramatic and  $\sin(x)$  function in eq. (6) is not very important at the present level of accuracy.

## 9 Discussion

In this section we will try to understand the observed  $x_A$ -scaling, which is approximated by eqs. (6) – (10), within the framework of the ideas of

existing models. We begin our discussion of the results with a set of rules which reproduce the known features of the data.

The analyzing power for hadron production, as well as hyperon polarization in inclusive reactions are proportional to an imaginary part of the product of spin-flip and spin-nonflip amplitudes

$$A_N \propto \text{Im}(f_{snf} f_{sf}^*) = |f_{snf}| |f_{sf}| \sin(\Delta\phi), \quad (14)$$

where  $\Delta\phi$  is a phase difference of the corresponding amplitudes [3, 15, 26]. The equality of  $\Delta\phi$  to zero means  $A_N = 0$ , so we may suggest that at  $x_A = x_0$  phase difference  $\Delta\phi = 0$  in case of  $\pi^+$ -meson production at high energy and  $p_T$ .

The sign of analyzing power at a quark level is given by the rule: A quark with spin *upward* prefers scattering to the *left*, and vice versa. Such result is easy to get by taking into account the interaction of a quark chromomagnetic momentum with chromomagnetic field, arising after the collision during hadronization [15]. This rule is also a direct consequence of the experimental observations [27].

The effect of recombination of partons in the proton while they transfer into an outgoing hadron may be different depending on whether they are accelerated (as with slow sea quarks) or decelerated (as with fast valence quarks). Slow partons mostly recombine with their spin downwards in the scattering plane while fast partons recombine with their spin upward [28].

The existence of the  $x_0$  point in eq. (6), where the analyzing power changes its sign, can be explained by the same arguments which are used to explain the  $x_F$ -dependence of  $\Lambda$ -hyperon polarization in the SU(6) based parton recombination model [28]. Following the same arguments we can say that the analyzing power for  $\Lambda$ -production is proportional to  $\Delta p$ -change in the momentum of sea  $s$ -quark:

$$\Delta p_S \propto 1/3(x_F - 3x_S), \quad (15)$$

where  $x_S \approx 0.1$  is a fraction of proton momentum, which carries sea  $s$ -quark. We assume here that the above rules concerning close relation of quark polarization and analyzing power of scattering are valid. Substituting  $x_F$  by  $x_A$ , we get the expression similar to eq. (6) with  $x_0 = 3x_S$  about 0.3, which agrees qualitatively with the experimental data (see Fig. 15) for the production analyzing power of  $\Lambda$ -hyperon, which is close to zero for  $0.2 \leq$

$x_A \leq 0.6$ . The only difference consists in the absence of  $\sin(x)$  function in eq. (15), which is not very essential since the analyzing power is small.

In case of  $\pi^+$ ,  $K^+$ -meson production we can apply similar arguments. In this case  $\Delta p$  for sea quark ( $\bar{d}$  or  $\bar{s}$ ) is equal to

$$\Delta p_{SEA} \propto 1/2(x_F - 2x_{SEA}), \quad (16)$$

and we again have the expression similar to eq. (6) with  $x_0 = 2x_{SEA}$  about 0.2 in agreement with the experimental data (see Table 1). An accelerated sea quark has spin downwards and recombines with a valence spin upward  $u$ -quark from a polarized proton, producing  $\pi^+$  or  $K^+$ -meson preferably to the left, which means a positive analyzing power. At  $x_A \leq x_0$ , the acceleration is replaced by the deceleration, which reverses the sea and valence quark spin directions and the analyzing power sign.

A dynamical reason for the above mentioned spin-momentum correlation is explained in [28] by the effect of Thomas precession [29, 30]. Another explanation of spin-momentum correlation follows from a picture of a colour flux tube, which emerges after the collision between an outgoing quark and the rest of hadronic system [15, 31].

The analyzing power of  $\pi^+$  production by polarized protons is determined by a product of the elementary subprocess analyzing power ( $A_q$  for polarized quark production), the polarization of this quark ( $P_q$ ), and a “dilution” factor due to the presence of other contributions, not related with the valence quark fragmentation [15]

$$A_N = A_q P_q \sigma(q) / (\sigma(q) + \sigma(g)). \quad (17)$$

The  $u$ -quark polarization according to SLAC [32], CERN [33] and DESY [34] measurements is positive and grows with a fraction of momentum carried by quark and in the first approximation can be taken as  $P_q = x_A$ , which is a generalization of  $P_q = x_F$ , assumed in [15]. For  $A_q$  we take the expression

$$A_q = \delta p_T \cdot 2p_T / (m^2 + p_T^2), \quad (18)$$

where  $\delta p_T$  ( $\sim 0.1$  GeV/c) is an additional transverse momentum, which quark with spin upward acquires in the chromomagnetic field of the flux tube, and  $m^2$  is some effective quark mass squared [15]. This expression for  $A_q$  is similar, in its functional form, to the lower order QCD calculations and gives

$A_N$  decreasing down to very small values at very high  $p_T$  [15, 16]. In our case (eq. (6))  $A_q$  is proportional to  $F(p_T)$ , given by eq. (7). The resulting expression for the  $A_N$  is

$$A_N = \delta p_T \cdot x_A \cdot 2p_T / (m^2 + p_T^2) D(x_A), \quad (19)$$

where  $D(x_A)$  is a “dilution” factor mentioned above. Eq. (19) is very similar to eq. (6) and to its high energy limit (11) with  $x_0 = 0$ . The distinction consists in numerical values of parameters in eqs. (19) and (6). In our case  $\delta p_T = c \cdot m \cdot \omega = 1.4 \text{ GeV}/c$ , and  $m = 2 \text{ GeV}$ , instead of  $m = 0.33 \text{ GeV}$  in [15]. We assume here that the “dilution” factor  $D(x_A)$  is close to unity at high  $x_A$  values. The values of the parameter  $m$ , obtained in [3] ( $m = 2 \text{ GeV}$ ) turned out to be much closer to that given in Table 1.

Another argument in favor of analyzing power and phase difference between spin-flip and spin-nonflip amplitudes to be proportional to hadron energy is given in [3, 35]. The reason is that the probability of quark spin-flip in an external field is proportional to a quark mean range before its hadronization. The experimental estimate of the hadronization range indicates that it is proportional to the secondary hadron energy [36].

We may conclude that eq. (6), which describes the scaling behaviour of analyzing powers, has a reasonable explanation of its basic components within the frameworks of existing models.

Summarizing the above discussion we may assume that the observed  $x_A$ -scaling takes place due to the dependence of phase difference of spin-flip and spin-nonflip amplitudes at high  $p_T$  and energy on  $x_A$  only. This dependence for production of some hadrons ( $\pi^+$ ,  $\pi^0$ ,  $K^\pm$ ,  $K_S^0$ ,  $\eta$ ,  $\bar{p}$ ) has a very simple form:

$$\Delta\phi \propto \omega(x_A - x_0). \quad (20)$$

The  $x_F$ -dependence (and hence the  $x_A$ -dependence) of the analyzing powers reflects in some models the corresponding dependence of the constituent quark polarization in the polarized proton [37].

The  $p_T$ -dependence of the analyzing power, given by eq. (7), reflects probably the ratio of spin-flip and spin-nonflip amplitudes [3]:

$$F(p_T) = 2p_T m / (m^2 + p_T^2) \propto \frac{|f_{snf}| |f_{sf}|}{|f_{snf}|^2 + |f_{sf}|^2}. \quad (21)$$

Both assumptions are not strictly proved, but they seem reasonable in view of the above stated arguments.

It is interesting to note that maximum of  $F(p_T)$  takes place at about the same  $p_T$ , where the dip in elastic  $p^\uparrow p$ -scattering exists and where the interference maximum of spin-flip and spin-nonflip amplitudes takes place [38].

A more detailed comparison of different model predictions with the scaling behaviour of the experimental analyzing power is the subject for a separate paper.

## 10 Possible application of inclusive reactions for the purpose of the beam polarimetry

A new generation of experiments with polarized proton beams requires a precise measurement of beam polarization. Unfortunately, above 100 GeV, the hadronic spin asymmetries used in most polarimeters are small and not well known.

The Coulomb-nuclear interference (CNI) method has a systematic uncertainty of the order of 10% due to contribution of unknown hadronic spin-flip amplitude [39]. The only experimental measurement of  $A_N$  in the CNI region ( $-t \leq 0.05 \text{ GeV}^2$ ) at 200 GeV has relative errors about 30% or more [40].

The analyzing power of the Coulomb coherent process (the Primakoff effect) has been measured at 185 GeV polarized beam [41]. Relative experimental errors for the analyzing power were 21% (statistical) and 34% (scale error due to the dilution factor), respectively.

Scaling properties of the analyzing power for the inclusive hadron production and its high value for some of reactions allow, in principle, to use them for the purpose of the beam polarimetry in a wide energy range. The most promising is the reaction of  $\pi^+$  production in  $p^\uparrow p$  or  $p^\uparrow A$  collisions, where  $A$  is a light nucleus. Kinematic region  $p_T \geq 1 \text{ GeV}/c$  and  $x_A \geq 0.5$  must be used to achieve a reasonable relative accuracy (15% or better). This accuracy is comparable with accuracy achieved using the analyzing power of elastic  $p^\uparrow p$  scattering, see for example [18]. The agreement of the data [18] on the carbon target with other data on the proton target in Figs. 3, 6 and 7 for  $p_T \geq 0.8 \text{ GeV}/c$  supports a possible use of light nuclei targets in polarimeters.

Other reactions with significant asymmetry in the region  $x_A \geq 0.5$  and  $p_T \geq 1$  GeV/c include  $\pi^-$  and  $\pi^0$  production in  $p^\uparrow p$  or  $p^\uparrow A$  collision. If a polarimeter is able to identify different hadrons then all of them can be used to measure beam polarization and to decrease errors, both statistical and systematic.

Further improvement of the analyzing power experimental accuracy will make such polarimeters competitive with other possibilities (e.g. the Primakoff effect, the elastic  $p^\uparrow p$  scattering, etc).

## 11 Scaling predictions for future experiments

The existence of the  $x_A$ -scaling is established from a limited set of data which cover only a restricted range of kinematic variables ( $p_T$ ,  $x_A$ , and  $\sqrt{s}$ ). The corresponding c.m. production angles are concentrated mostly near  $0^\circ$ ,  $90^\circ$ , and  $180^\circ$ . A more detailed study of  $p_T$ ,  $x_A$ , and energy dependences could clarify theoretical basis for the  $x_A$ -scaling and help to compare it with various models.

Detailed predictions of  $A_N$  dependence on  $x_A$  for  $\pi^+$ -production at various laboratory angles in  $p^\uparrow p$  collisions at 40 GeV/c are shown in Fig. 23. This dependence is given by eqs. (6)–(10) with the parameters presented in Table 1. The measurements can be carried out at the FODS-2 experimental setup in IHEP (Protvino) which uses a 40 GeV/c polarized proton beam [2]. As is seen from Fig. 23, the asymmetry is negative for the  $x_A$  near 0.08 and grows in absolute value with the increase of laboratory angle. At  $x_A = 0.19$   $A_N$  is always equal to zero and can be used to check systematic errors in the asymmetry measurements. The largest values of  $A_N$  are reached for laboratory angle near 70 mrad. At this angle the values of  $x_A$  and  $A_N$  could be larger than 0.8 and 0.4, respectively. At smaller angles and large  $x_A$ , the asymmetry is smaller owing to the decrease of  $p_T$  and the corresponding reduction of the function  $F(p_T)$  (see eq. (7)).

The dependence of  $A_N$  for the  $\pi^+$  production in  $p^\uparrow p$  collisions at 40 GeV/c on  $p_T$  at several values of  $x_A$  is shown in Fig. 24. It is possible to measure not only the rise of  $A_N$  for  $0 \leq p_T \leq 2$  GeV/c, but also its probable decrease at higher  $p_T$  even at 40 GeV beam energy. For the  $x_A$  values near 0.6, we can measure the shape of  $p_T$ -dependence up to 4 GeV/c. Much higher  $p_T \leq 10$  GeV/c can be reached at 200 GeV, where  $A_N$  could decrease significantly (if

there is no plateau at high  $p_T$ ) in comparison with its maximum value at  $p_T$  about 2 GeV/c.

The  $A_N$  dependence for the  $\pi^+$  production in  $p^\uparrow p$  collisions on  $x_A$  at different beam energies and  $p_T = 0.5$  GeV/c is shown in Fig. 25. The corresponding parameters are taken from Table 1. As is seen in Fig. 25, the asymmetry approaches its high energy limit for the  $E^{BEAM} \geq 70$  GeV. At smaller energies in the range from 10 to 40 GeV and the low  $p_T$  value, there is a significant contribution of nonasymptotic term (eq. (8)), which is most prominent at  $x_A = 0.75$ , and changes the form of  $x_A$ -dependence. For energies above 70 GeV the contribution of eq. (8) is practically negligible.

The oscillation of  $A_N$  as a function of  $x_A$  is predicted for the  $\pi^0$  and  $\eta$ -meson production in  $\pi^- p^\uparrow$ -collisions (see Figs. 21 and 22).

It is worth noticing that the expected maximum of  $|A_N|$  for the  $K^+$ -meson production in  $p^\uparrow p$ -collisions is smaller than it is for the  $\pi^+$ -meson production. It could be related to a higher mass of constituent  $\bar{s}$ -quark as compared with  $\bar{d}$ -quark mass. The higher constituent quark mass leads to a smaller chromomagnetic momentum ( $\mu \propto 1/m_q$ ) and a smaller asymmetry [15].

A high value of  $A_N$  is expected for the  $p^\uparrow p \rightarrow K^- + X$  reaction at large  $x_A$  (see Table 5) which contradicts some models that predict zero asymmetry [42].

We can make predictions for other reactions, using eqs. (6)–(13) and the parameters, presented in Tables 1 – 8.

## 12 Conclusions

It is shown that the existing analyzing power data in inclusive reactions for meson ( $\pi^\pm$ ,  $K^\pm$ ,  $K_S^0$ ,  $\eta$ ) and baryon ( $p$ ,  $\bar{p}$ ,  $\Lambda$ ) productions in  $p^\uparrow p(A)$ - and  $\bar{p}^\uparrow p(A)$ -collisions can be described by a simple function of three variables ( $\sqrt{s}$ ,  $p_T$ ,  $x_A$ ), where  $x_A = E/E^{BEAM}$  is a new scaling variable. In the limit of high enough energy ( $E^{BEAM} \geq 40$  GeV) and high  $p_T$  ( $p_T \geq 1.0$  GeV/c),  $A_N$  is a function of  $x_A$  and  $p_T$  only with a precision of about 0.02–0.06, depending on the reaction type. A simple expression  $A_N = F(p_T)G(x_A)$  can be used to approximate the experimental analyzing powers in the above range of high energies and  $p_T$ . This scaling behaviour is better fulfilled for the  $\pi^+$ ,  $\pi^0$ ,  $K^+$ ,  $\eta$ , and  $\Lambda$ -production in  $p^\uparrow p$ -collisions, which takes place probably at the quark level. The most solid experimental conformation of the  $x_A$ -scaling exists now

for  $\pi^+$  production in  $p^\dagger p(A)$ -collisions, where 6 independent measurements have been performed in a wide range of  $p_T$ ,  $x_A$ , and  $\sqrt{s}$ .

Significant non-asymptotic (energy dependent) contributions are observed for the  $\pi^-$  and proton production. The former has a noticeable gluon contribution, and the latter can be produced mainly from protons, existing in the initial state.

The analyzing power for some reactions has not yet been explored thoroughly enough to make a conclusion about the  $x_A$ -scaling features. The additional  $A_N$ -measurements are necessary at several c.m. angles in the central and fragmentation regions and at different energies. The bin size in  $x_A$  and  $p_T$  should be small enough to get one unbiased averaging over it, and to estimate mean values of  $x_A$  and  $p_T$  for each data point. In an ideal case, new experiments should measure  $x_A$ -dependence at fixed  $p_T$  and  $p_T$ -dependence at fixed  $x_A$ . Of interest is also a high  $p_T$ -region ( $2 \leq p_T \leq 10$  GeV/c), where the decrease of the analyzing power is expected with a  $p_T$  rise according to some models [15, 16, 42].

The asymptotic dependence of  $A_N$  on  $x_A$  for most of the hadrons has a characteristic point  $x_0$ , where it intersects zero and probably changes its sign. Such behaviour is in a qualitative agreement with the predictions from the models which take into account the Thomas precession and chromomagnetic forces between an outgoing quark and the rest of hadronic system. The linear dependence of  $A_N$  on  $x_A$  for most of the reactions may indicate that the polarization of a valence quark, which is kicked out from a proton and fragments into a hadron  $h$ , containing this quark, is proportional to  $x_A$  or to the secondary hadron energy.

The use of eqs. (6) – (13) with the known parameters allows one to predict  $A_N$  in a wide range of kinematic variables and to use these predictions for the comparison with the models, to optimize future experiments and to use some reactions as polarimeters.

## References

- [1] D.L. Adams et al., *Phys. Lett. B* **264** (1991) 462.
- [2] V.V. Abramov et al., *Nucl. Phys. B* **492** (1997) 3, hep-ex/0110011.
- [3] N.S. Amaglobeli et al., *Yad. Fiz.* **50** (1989) 695. [*Sov. J. Nucl. Phys.* **50** (1989) 432].
- [4] V.D. Apokin et al., *Yad. Fiz.* **49** (1989) 156 [*Sov. J. Nucl. Phys.* **49** (1989) 97].
- [5] V.D. Apokin et al., *Phys. Lett. B* **243** (1990) 461.
- [6] A. Bravar et al., *Phys. Rev. Lett.* **77** (1996) 2626.
- [7] D.L. Adams et al., *Phys. Rev. D* **53** (1996) 4747.
- [8] D.L. Adams et al., *Z.Phys. C* **56** (1992) 181.
- [9] S. Saroff et al., *Phys. Rev. Lett.* **64** (1990) 995.
- [10] N.I. Belikov et al., *Preliminary results on raw asymmetry in the  $\pi^0$ -production on a polarized target at 70 GeV*. IHEP preprint 97-51, Protvino, 1997;  
N.I. Belikov et al., *In Proc. of the 13th International Symposium on High Energy Spin Physics*, Sept. 8-12, Protvino, 1998, (Protvino, Russia, 1999). Edited by N.E.Tyurin et al., p. 465.
- [11] J. Antille et al., *Phys. Lett. B* **94** (1980) 523.
- [12] W.H. Dragoset et al., *Phys. Rev. D* **18** (1978) 3939.
- [13] I.G. Alekseev et al., *Nucl. Instr. and Meth. A* **434** (1999) 254.
- [14] D.G. Aschman et al., *Nucl. Phys. B* **142** (1978) 220.
- [15] M.G. Ryskin, *Yad. Fiz.* **48** (1988) 1114 [*Sov. J. Nucl. Phys.* **48** (1988) 708].
- [16] G. Kane, J. Pumplin, and W. Repko, *Phys. Rev. Lett.* **41** (1978) 1689.

- [17] D.L. Adams et al., *Nucl. Phys.* **B 510** (1998) 3.
- [18] C. Allgower et al., *Measurement of single-spin asymmetries of  $\pi^+$ ,  $\pi^-$ , and protons inclusively produced on a carbon target with a 21.6 GeV/c incident polarized proton beam (BNL E925 Experiment)*. IHEP preprint 99-14, Protvino, 1999; (SCAN-9909048)  
K. Krueger et al., *Phys. Lett.* **B 459** (1999) 412.
- [19] M.V. Tokarev, G.P. Skoro, *On polarization mechanism in inclusive meson production and asymmetry sign rule*. JINR Preprint E2-95-50, Dubna 1995. (SCAN-9604096)  
G.J. Musulmanbekov, M.V. Tokarev, *Simulation of single spin asymmetry in  $p^\uparrow p \rightarrow \pi^{\pm 0} X$  reactions*. In Proc. of the 6th Workshop on High Energy Spin Physics, Protvino, 1995. Edited by S.B. Nurushev et al., (Protvino, Russia, 1996). Vol. 1, p. 132. (SCAN-9604097)
- [20] D.S. Ayres et al., *Phys. Rev.* **D 15** (1977) 1826.
- [21] B.E. Bonner et al., *Phys. Rev. Lett.* **61** (1988) 1918.
- [22] D.L. Adams et al., *Phys. Lett.* **B 261** (1991) 201.
- [23] B.E. Bonner et al., *Phys. Rev.* **D 38** (1988) 729.
- [24] A. Bravar et al., *Phys. Rev. Lett.* **75** (1995) 3073.
- [25] B.E. Bonner et al., *Phys. Rev.* **D 41** (1990) 13.
- [26] N.S. Craigie et al., *Phys. Rep.* **99** (1983) 69.
- [27] Liang Zuo-tang and C. Boros, *Phys. Rev. Lett.* **79** (1997) 3608.
- [28] T.A. DeGrand, H. Miettinen, *Phys. Rev.* **D 24** (1981) 2419.
- [29] L.T. Thomas, *Philos. Mag.* **3** (1927) 1.
- [30] A.A. Logunov, *On Tomas Precession*. IHEP preprint 98-85, Protvino, 1998.
- [31] B. Anderson, G. Gustafson and G. Ingelman, *Phys. Lett.* **B 85** (1979) 417; *Phys. Rep.* **97** (1983) 31.

- [32] SLAC/E143 Collaboration, K. Abe et al., *Phys. Rev. D* **58** (1998) 112003.
- [33] SMC Collaboration, D. Adeva et al., *Phys. Lett. B* **420** (1998) 180; *Phys. Rev. D* **58** (1998) 112001.
- [34] HERMES Collaboration, A. Airapetian et al., *Phys. Lett. B* **442** (1998) 484; K. Ackerstaff et al., *Phys. Lett. B* **464** (1999) 123.
- [35] Yu. Arestov, in *Proceedings of the 12th International Symposium on Spin Physics*, Amsterdam, 1996 (World Scientific, Singapore, 1997), p. 187.
- [36] V.V. Abramov, *Yad. Fiz.* **44** (1986) 1318 [*Sov. J. Nucl. Phys.* **44** (1986) 856].
- [37] S.M. Troshin and N.E. Tyurin, *Phys. Rev. D* **54** (1996) 838.
- [38] G. Fidecaro et al., *Phys. Lett. B* **105** (1981) 309.
- [39] N.H. Buttmore et al., *The spin dependence of high energy proton scattering*. Preprint CPT-98/P.3693, Marseille, France, 1998. (hep-ph/9901339)  
B.Z. Kopeliovich, *High-Energy Polarimetry at RHIC*. Preprint MPI H-V3-1998, Heidelberg, Germany, 1998. (hep-ph/9801414)
- [40] D.L. Adams et al., *Phys. Lett. B* **264** (1991) 462.
- [41] D.C. Carey et al., *Phys. Rev. Lett.* **64** (1990) 357.
- [42] M. Anselmino, M. Boglione and F. Murgia, *Phys. Lett. B* **362** (1995) 164.

## List of Figures

1	$A_N$ vs $p_T$ for the $\pi^+$ production by polarized protons. The curves correspond to a fit by eqs. (6–10) with the parameters given in Table 1. . . . .	31
2	$A_N$ vs $x_R$ for the $\pi^+$ production by polarized protons. The curves correspond to a fit by eqs. (6–10) with the parameters given in Table 1. . . . .	32
3	$A_N$ vs $x_A$ for the $\pi^+$ production by polarized protons. The curves correspond to a fit by eqs. (6–10) with the parameters given in Table 1. . . . .	33
4	$A_N$ vs $x_A$ for the $\pi^+$ production by polarized 11.75 GeV/c protons [12]. Dotted and dashed curves correspond to a fit by eqs. (6–10) for the regions $0.4 \leq p_T \leq 0.5$ and $0.9 \leq p_T \leq 1.2$ GeV/c, respectively. . . . .	34
5	$A_N$ vs $p_T$ for the $\pi^+$ production by polarized 11.75 GeV/c protons [12]. The curve corresponds to a fit by eqs. (6–10) for the $p^\pi = 8$ GeV/c. . . . .	35
6	The ratio $A_N/F(p_T)$ vs $x_A$ for the $\pi^+$ production by polarized protons. The curves correspond to a fit by eqs. (6–10) with the parameters given in Table 1. . . . .	36
7	$A_N$ vs $x_A$ for the $\pi^-$ production by polarized protons. The curves correspond to a fit by eqs. (6–10) with the parameters given in Table 2. . . . .	37
8	$A_N$ vs $x_A$ for the $\pi^-$ production by polarized 11.75 GeV/c protons [12]. The dashed and dotted curves correspond to a fit by eq. (6–10) for the regions $0.3 \leq p_T \leq 0.4$ and $0.5 \leq p_T \leq 0.6$ GeV/c, respectively. . . . .	38
9	$A_N$ vs $p_T$ for the $\pi^-$ production by polarized 11.75 GeV/c protons [12]. The curve corresponds to a fit by eqs. (6–10) for the $p^\pi = 8$ GeV/c. . . . .	39
10	$A_N$ vs $x_A$ for the proton production by polarized protons. The solid fitting curve corresponds to the 40 GeV/c data [2]. The dotted curve corresponds to the 13.3 GeV/c data [9]. The dashed curve corresponds to the 6 GeV/c data [20]. The dash-dotted curve corresponds to the 21.6 GeV/c data [18]. . . . .	40

11	$A_N$ vs $x_A$ for the $\pi^0$ production by polarized protons. The fitting curve corresponds to the 200 GeV/c data [8]. . . . .	41
12	$A_N$ vs $x_A$ for the $K^+$ production by polarized protons. The solid fitting curve corresponds to the 40 GeV/c data [2], and the dashed curve corresponds to the 11.75 GeV/c data [12] and $0.5 \leq p_T \leq 0.6$ GeV/c. . . . .	42
13	The ratio $A_N/F(p_T)$ vs $x_A$ for the $K^-$ production by polarized protons. The solid fitting curve corresponds to the data [2], and the dashed curve corresponds to the data [12] and region $0.3 \leq p_T \leq 0.4$ GeV/c. . . . .	43
14	$A_N$ vs $x_A$ for antiproton production by polarized protons. The curve corresponds to a fit by eq. (6) with the parameters given in Table 5. . . . .	44
15	$A_N$ vs $x_A$ for the $\Lambda$ production by polarized protons. The solid fitting curve corresponds to the 18.5 GeV/c data [23], and the dashed curve corresponds to the 200 GeV/c data [24]. . . . .	45
16	$A_N$ vs $x_A$ for the $K_S^0$ production by polarized protons. The fitting curve corresponds to the 18.5 GeV/c data [23]. . . . .	46
17	$A_N$ vs $x_A$ for the $\eta$ production by polarized protons. The curve corresponds to a fit (6) with the parameters given in Table 7. .	47
18	$A_N$ vs $x_A$ for the $\pi^+$ production in $\bar{p}^\uparrow p$ -collisions. The curve corresponds to a fit by eq. (6) with the parameters given in Table 9. . . . .	48
19	$A_N$ vs $x_A$ for the $\pi^-$ production in $\bar{p}^\uparrow p$ -collisions. The curve corresponds to a fit by eq. (6) with the parameters given in Table 9. . . . .	49
20	$A_N$ vs $x_A$ for the $\pi^0$ production in $\bar{p}^\uparrow p$ -collisions. The fitting curve corresponds to the 200 GeV/c data [22]. . . . .	50
21	$A_N$ vs $x_A$ for the $\pi^0$ production in $\pi^- p^\uparrow$ -collisions. The solid curve corresponds to a fit by eq. (6) with the parameters given in Table 8. The dashed curve corresponds to an extrapolation of the fit (6) for the region $p_T=1$ GeV/c and $0.03 \leq x_A \leq 0.1$ . The dash-dot curve corresponds to an extrapolation of the fit (6) for the region $p_T=2$ GeV/c and $x_A \geq 0.3$ . . . . .	51

22	$A_N$ vs $x_A$ for the $\eta$ production in $\pi^- p^\uparrow$ -collisions. The solid curve corresponds to a fit by eq. (6) with the parameters given in Table 8. The dashed curve corresponds to an extrapolation of the fit (6) for the region $p_T=1$ GeV/c and $x_A \leq 0.15$ . The dash-dot curve corresponds to an extrapolation of the fit (6) for the region $p_T=2$ GeV/c and $x_A \geq 0.3$ . . . . .	52
23	Predictions of the $A_N$ vs $x_A$ for the $\pi^+$ production by polarized 40 GeV/c protons at the different laboratory angles. . . . .	53
24	Predictions of the $A_N$ vs $p_T$ for the $\pi^+$ production by polarized 40 GeV/c protons at the different $x_A$ values. . . . .	54
25	Predictions of the $A_N$ vs $x_A$ for the $\pi^+$ production by polarized protons at the different beam energies and $p_T = 0.5$ GeV/c. .	55

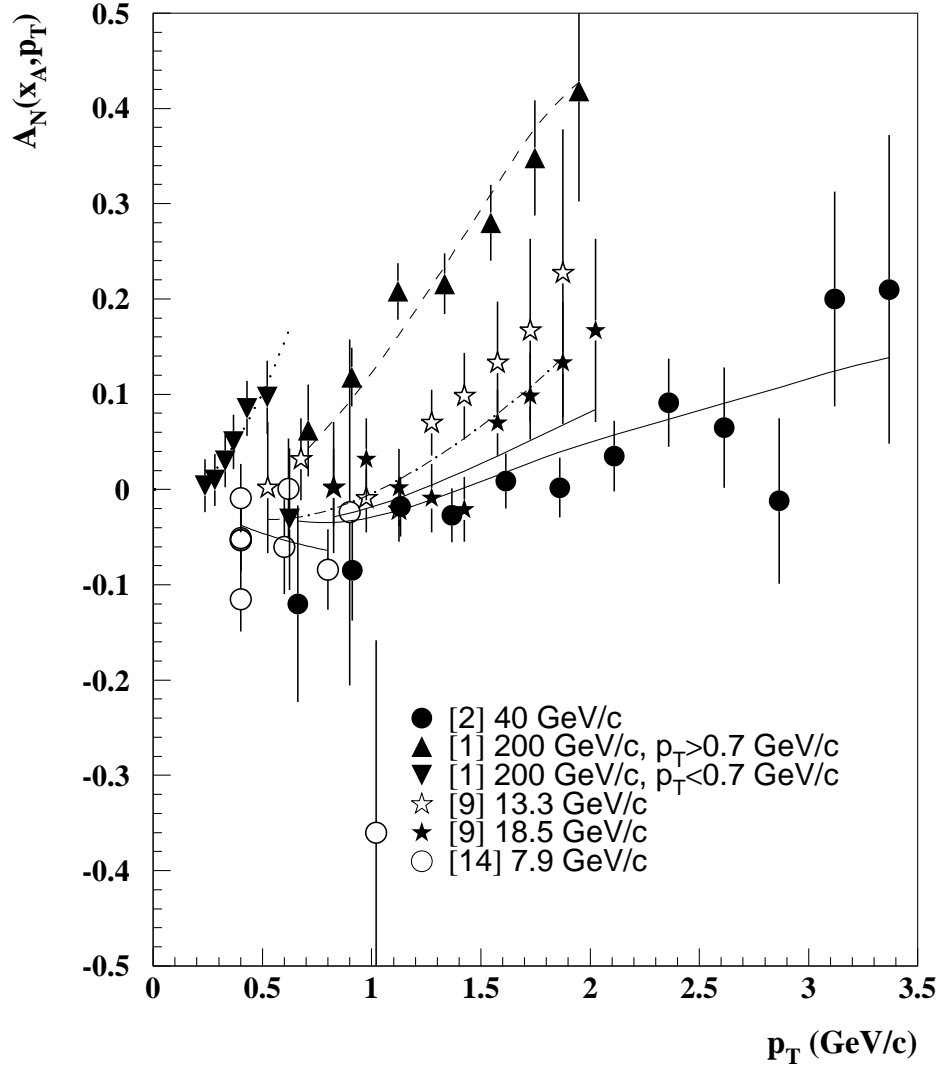


Figure 1:  $A_N$  vs  $p_T$  for the  $\pi^+$  production by polarized protons. The curves correspond to a fit by eqs. (6–10) with the parameters given in Table 1.

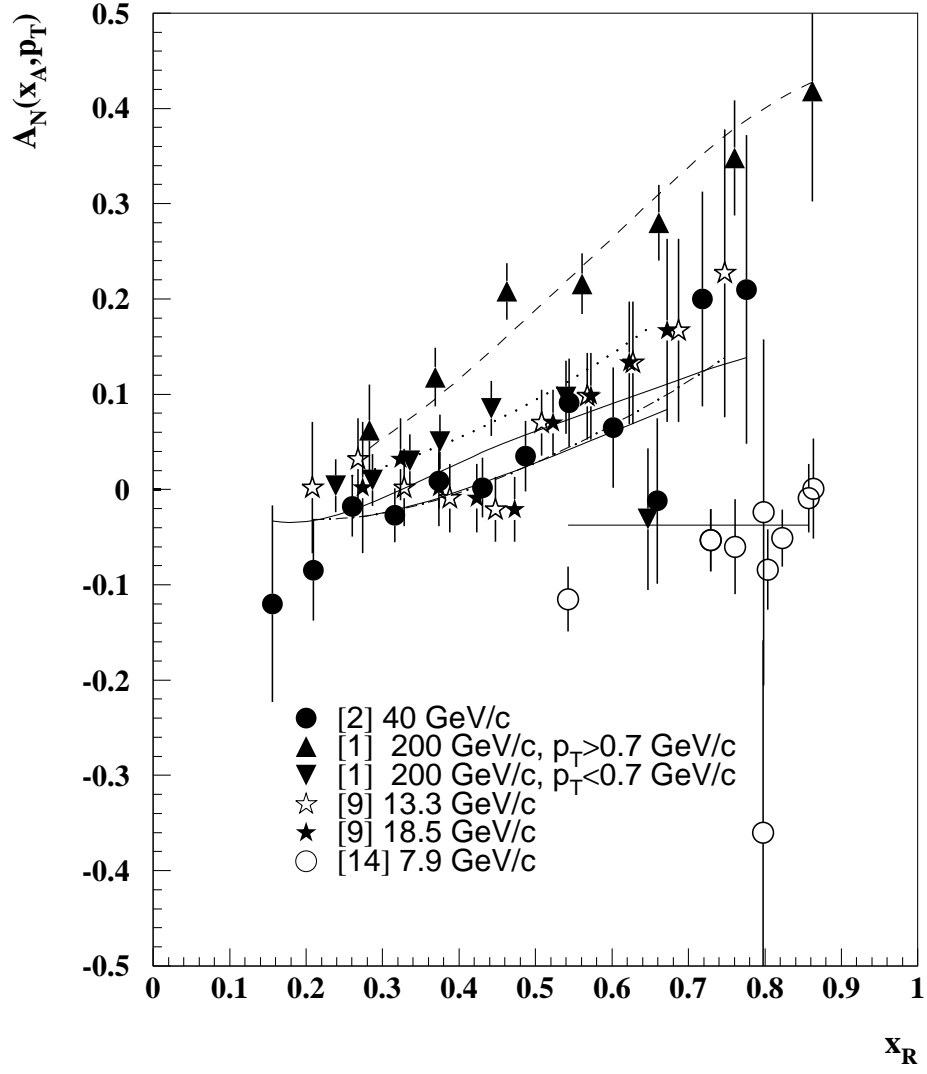


Figure 2:  $A_N$  vs  $x_R$  for the  $\pi^+$  production by polarized protons. The curves correspond to a fit by eqs. (6–10) with the parameters given in Table 1.

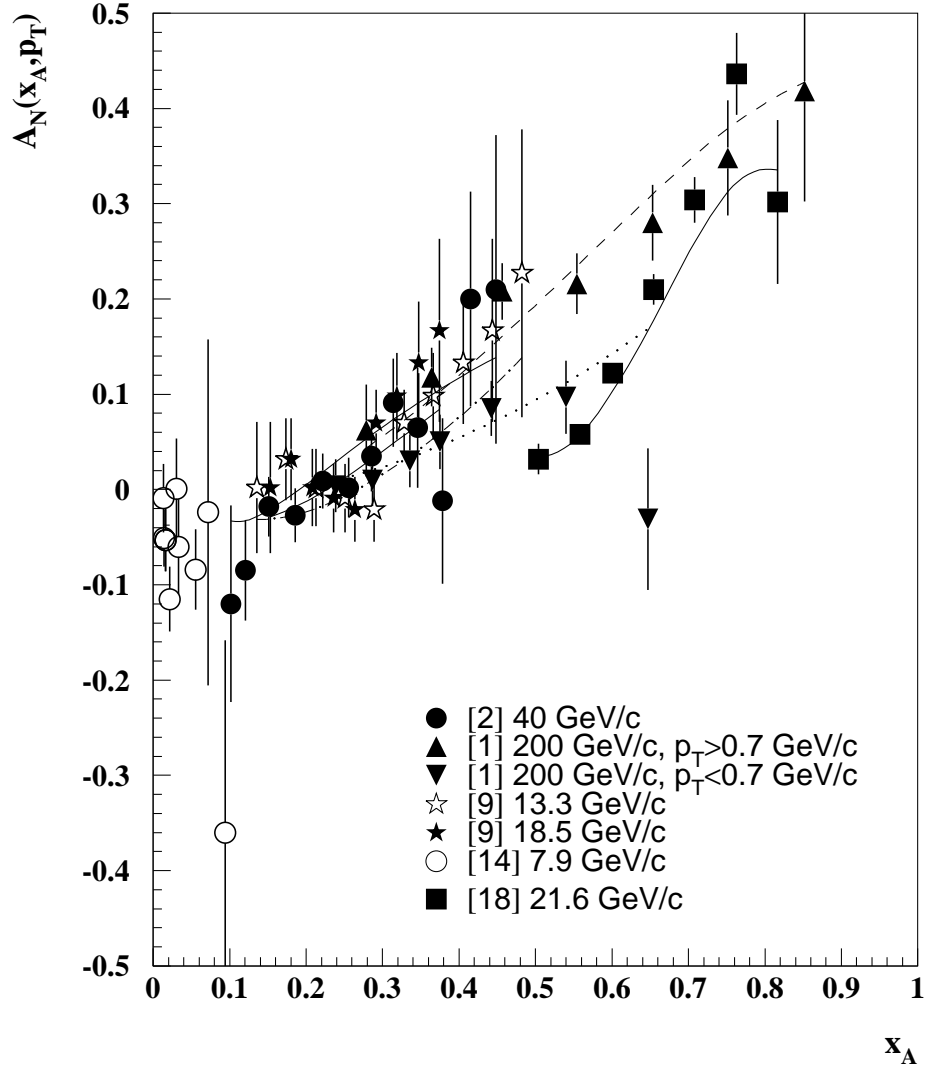


Figure 3:  $A_N$  vs  $x_A$  for the  $\pi^+$  production by polarized protons. The curves correspond to a fit by eqs. (6–10) with the parameters given in Table 1.

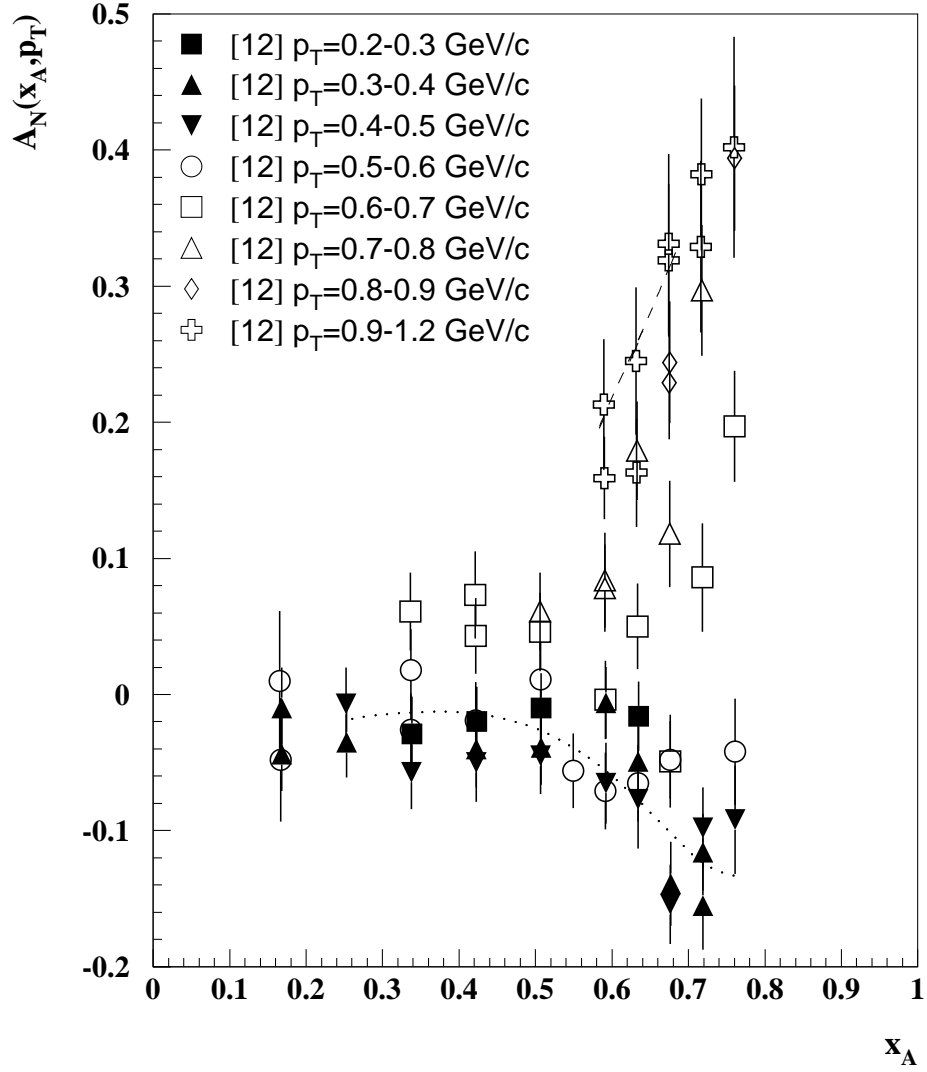


Figure 4:  $A_N$  vs  $x_A$  for the  $\pi^+$  production by polarized 11.75 GeV/c protons [12]. Dotted and dashed curves correspond to a fit by eqs. (6–10) for the regions  $0.4 \leq p_T \leq 0.5$  and  $0.9 \leq p_T \leq 1.2$  GeV/c, respectively.

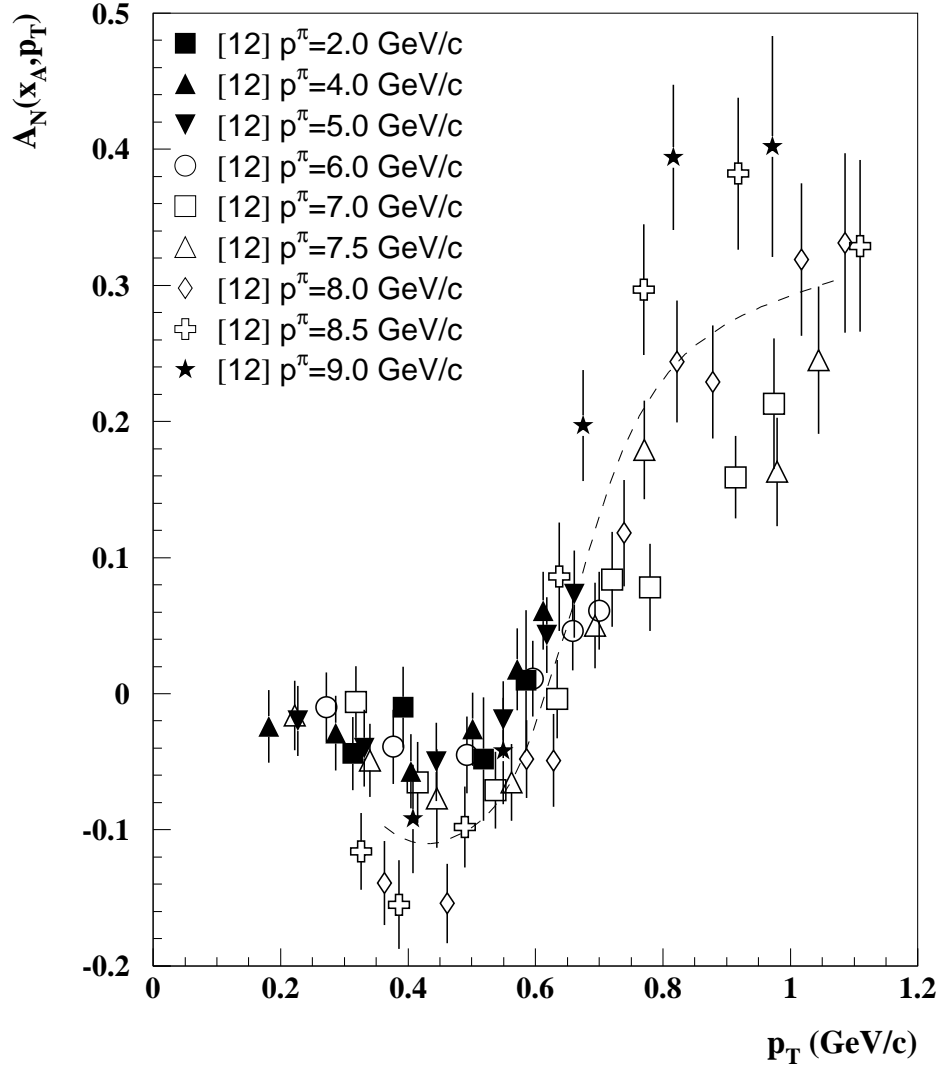


Figure 5:  $A_N$  vs  $p_T$  for the  $\pi^+$  production by polarized 11.75 GeV/c protons [12]. The curve corresponds to a fit by eqs. (6–10) for the  $p^\pi = 8$  GeV/c.

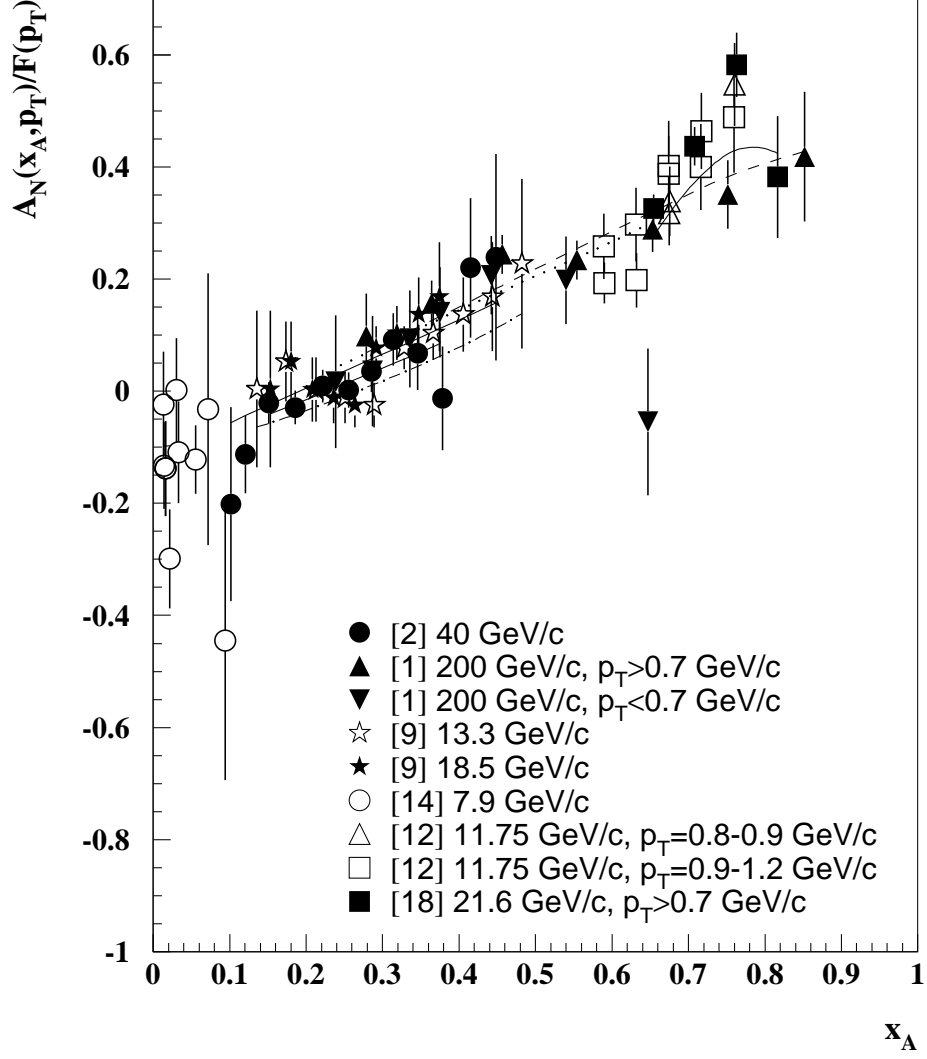


Figure 6: The ratio  $A_N/F(p_T)$  vs  $x_A$  for the  $\pi^+$  production by polarized protons. The curves correspond to a fit by eqs. (6–10) with the parameters given in Table 1.

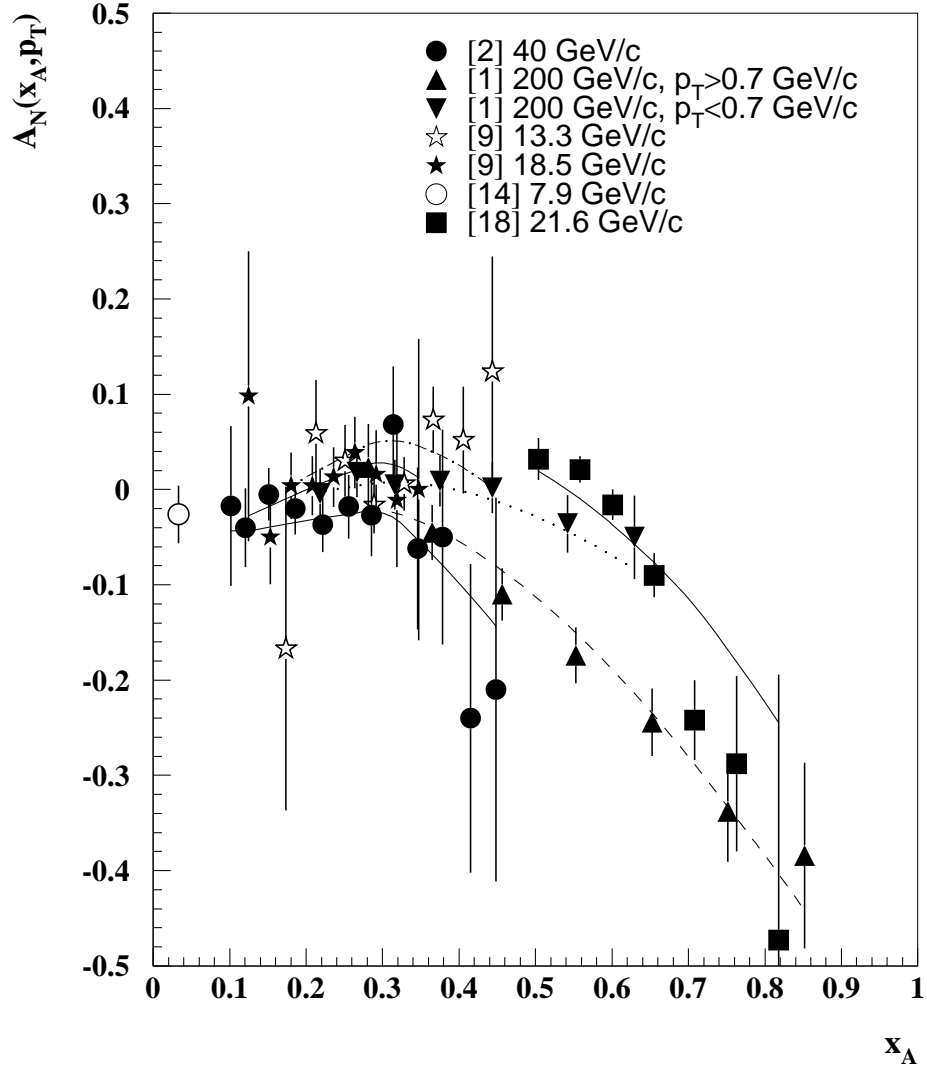


Figure 7:  $A_N$  vs  $x_A$  for the  $\pi^-$  production by polarized protons. The curves correspond to a fit by eqs. (6–10) with the parameters given in Table 2.

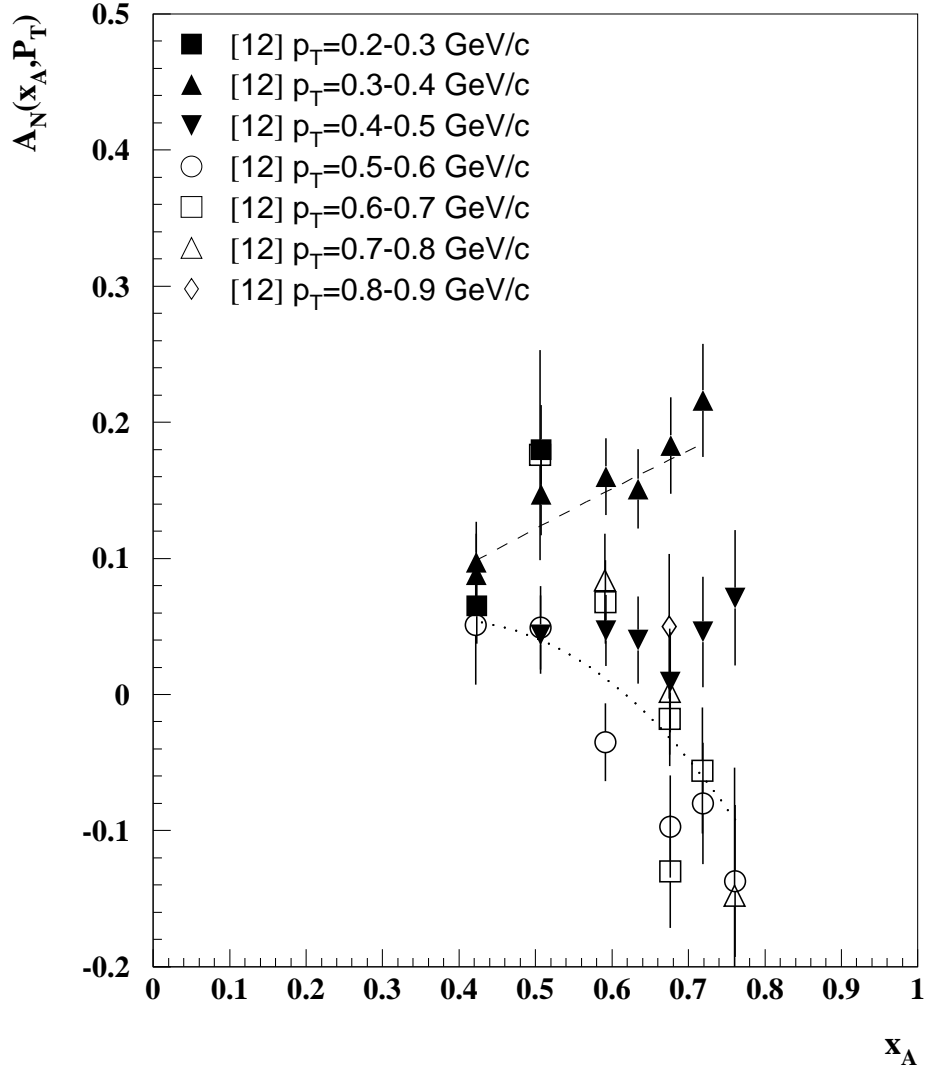


Figure 8:  $A_N$  vs  $x_A$  for the  $\pi^-$  production by polarized 11.75 GeV/c protons [12]. The dashed and dotted curves correspond to a fit by eq. (6–10) for the regions  $0.3 \leq p_T \leq 0.4$  and  $0.5 \leq p_T \leq 0.6$  GeV/c, respectively.

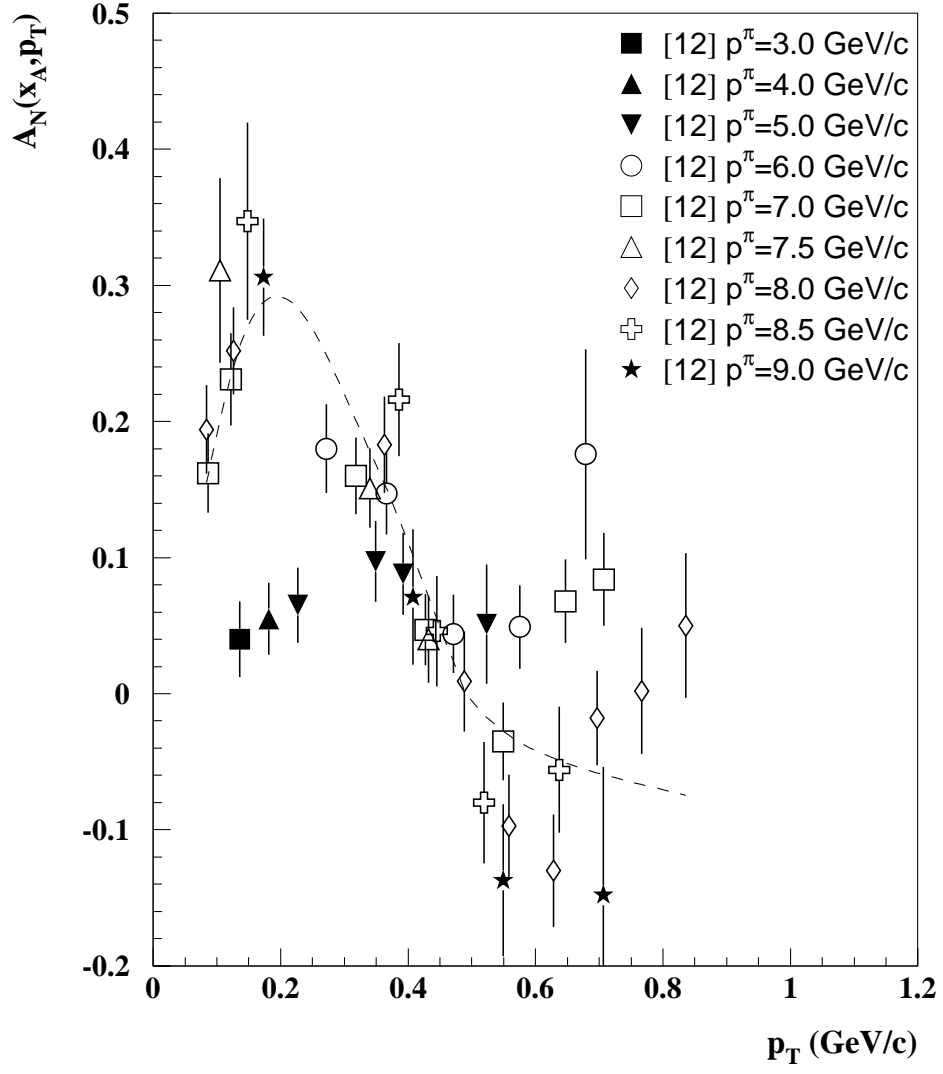


Figure 9:  $A_N$  vs  $p_T$  for the  $\pi^-$  production by polarized 11.75 GeV/c protons [12]. The curve corresponds to a fit by eqs. (6–10) for the  $p^\pi = 8$  GeV/c.

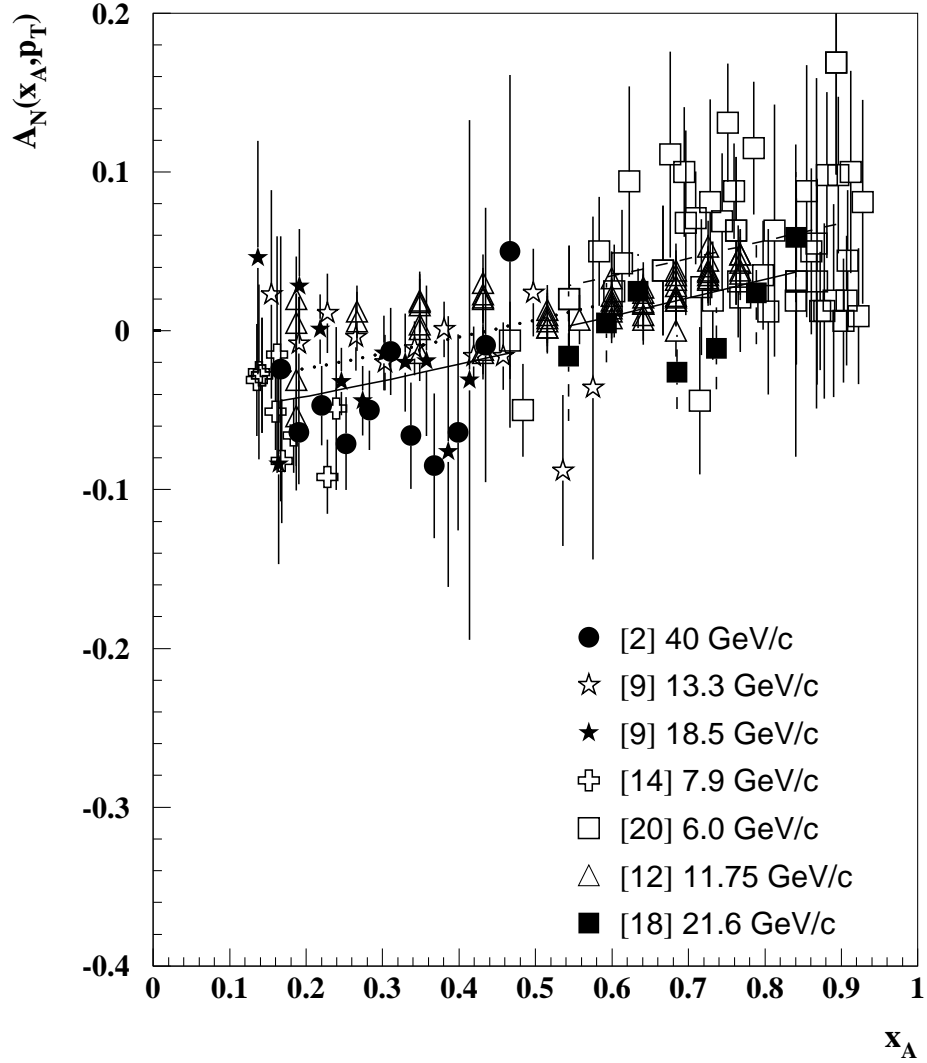


Figure 10:  $A_N$  vs  $x_A$  for the proton production by polarized protons. The solid fitting curve corresponds to the 40 GeV/c data [2]. The dotted curve corresponds to the 13.3 GeV/c data [9]. The dashed curve corresponds to the 6 GeV/c data [20]. The dash-dotted curve corresponds to the 21.6 GeV/c data [18].

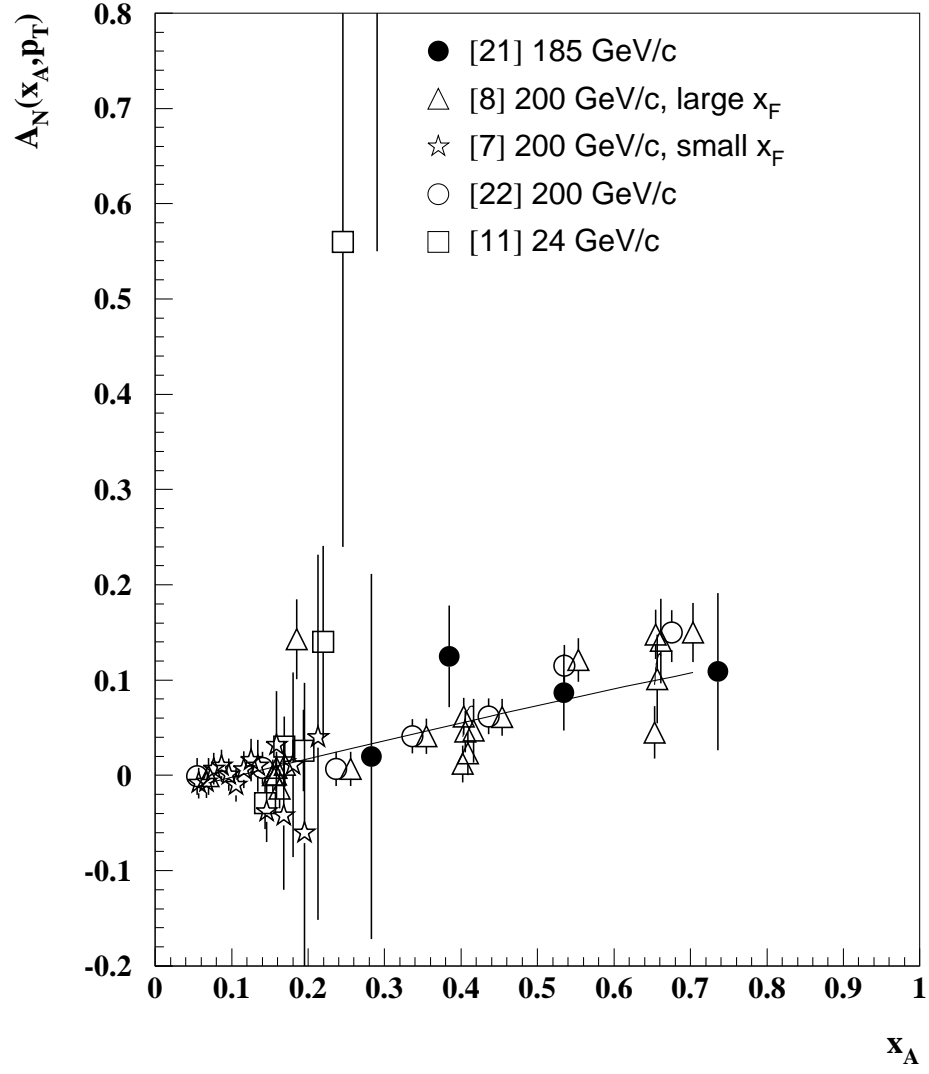


Figure 11:  $A_N$  vs  $x_A$  for the  $\pi^0$  production by polarized protons. The fitting curve corresponds to the 200 GeV/c data [8].

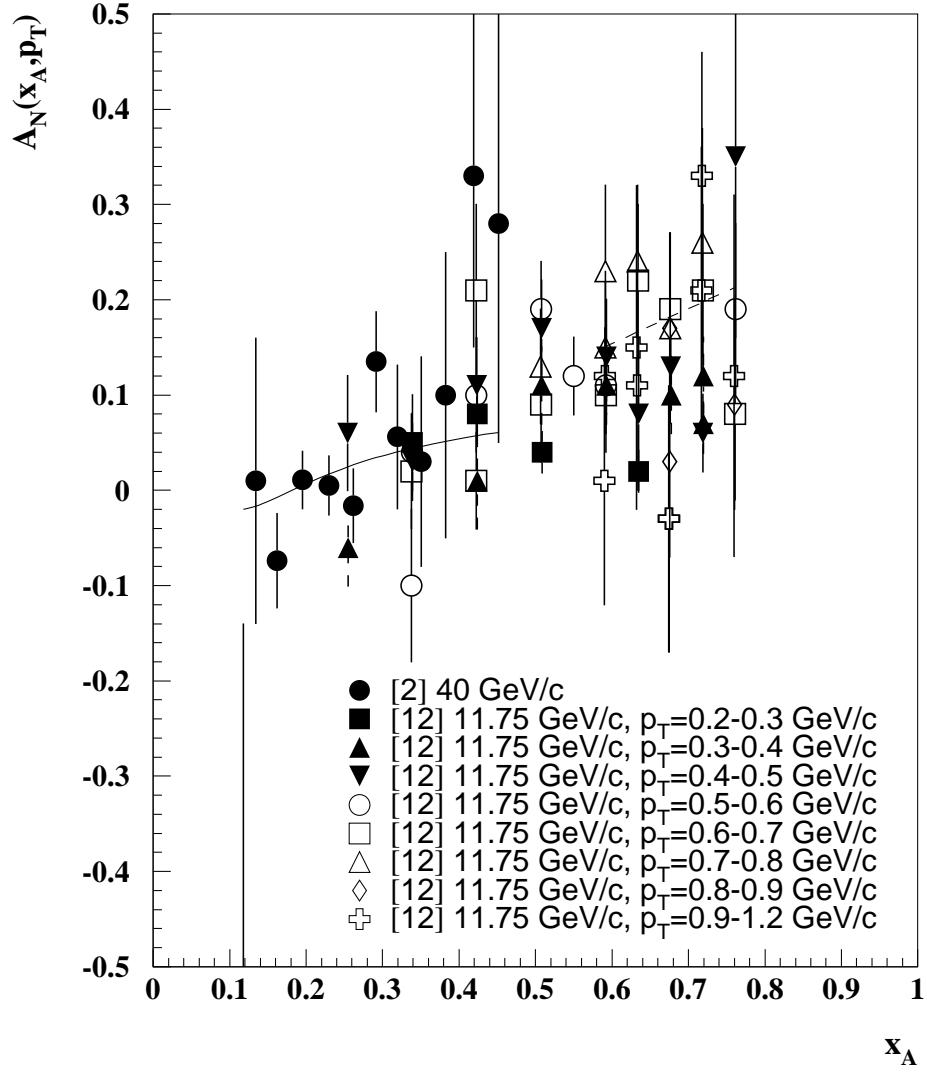


Figure 12:  $A_N$  vs  $x_A$  for the  $K^+$  production by polarized protons. The solid fitting curve corresponds to the 40 GeV/c data [2], and the dashed curve corresponds to the 11.75 GeV/c data [12] and  $0.5 \leq p_T \leq 0.6$  GeV/c.

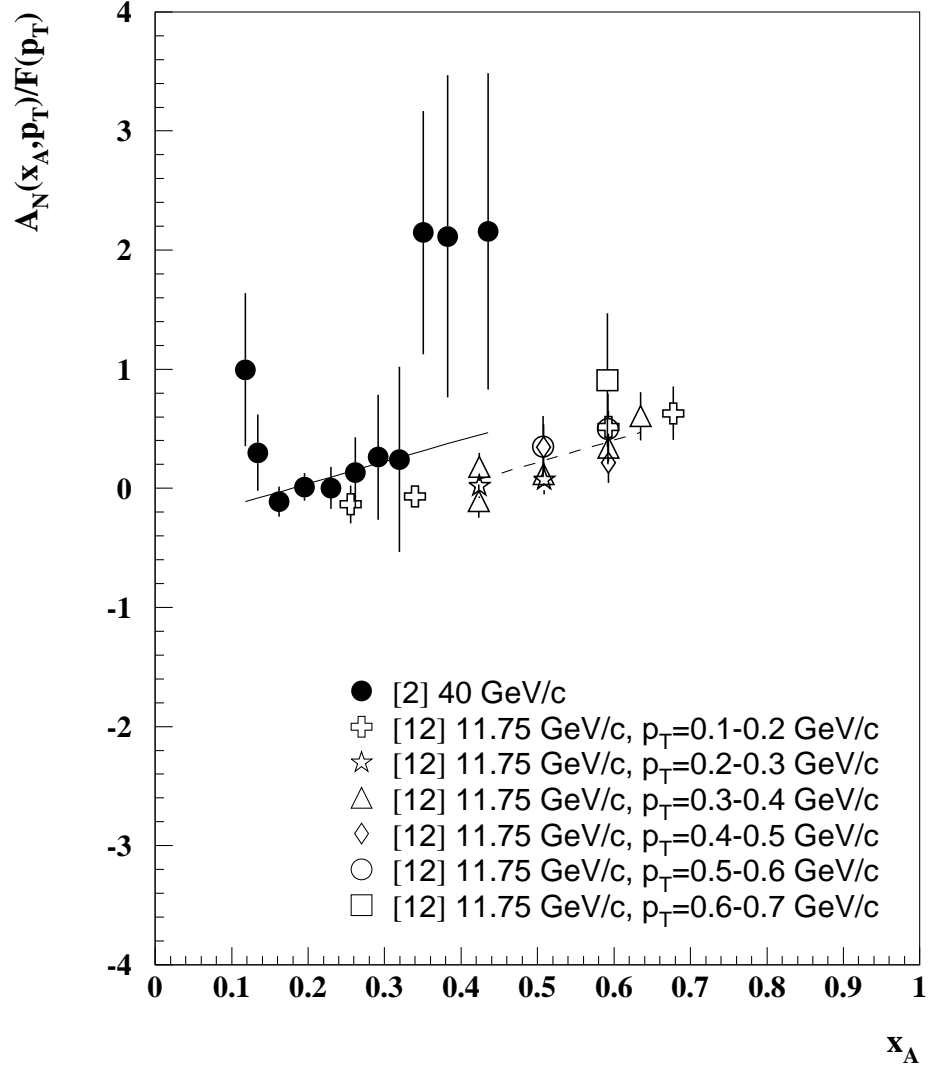


Figure 13: The ratio  $A_N/F(p_T)$  vs  $x_A$  for the  $K^-$  production by polarized protons. The solid fitting curve corresponds to the data [2], and the dashed curve corresponds to the data [12] and region  $0.3 \leq p_T \leq 0.4$  GeV/c.

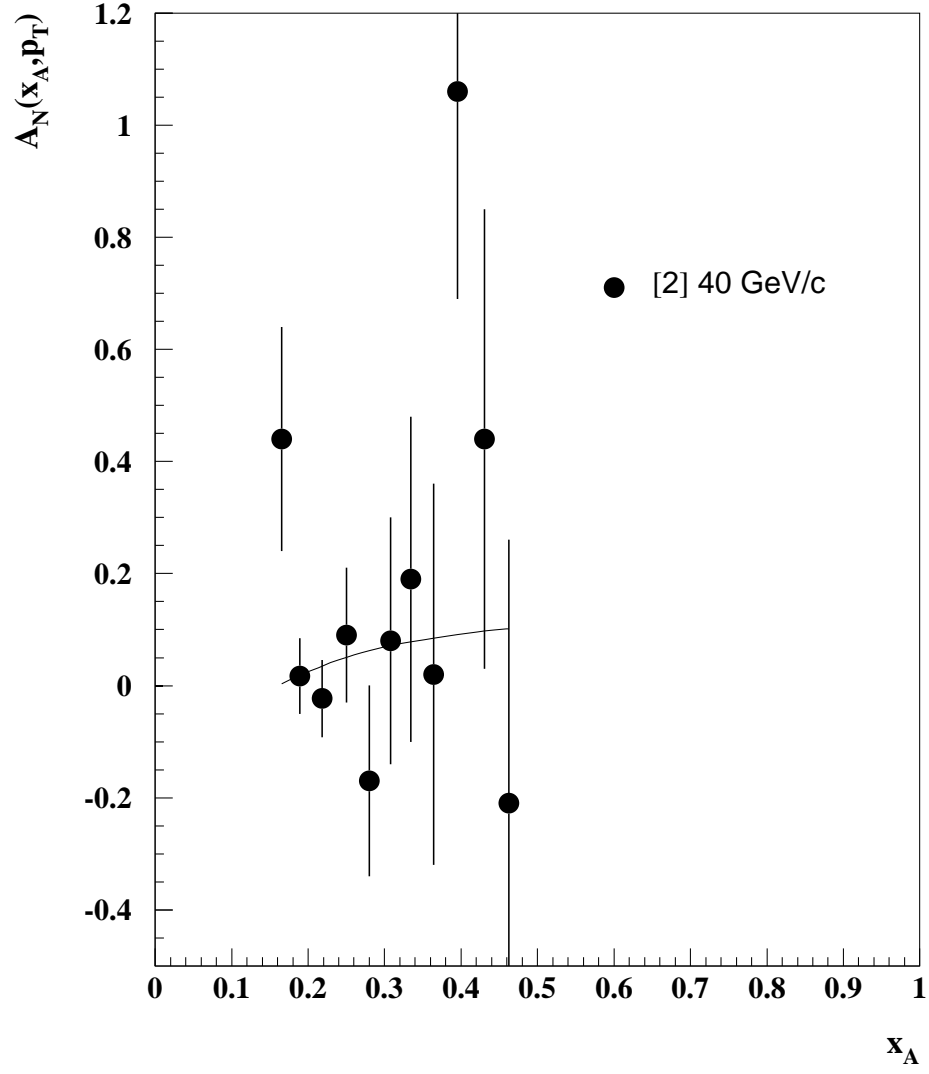


Figure 14:  $A_N$  vs  $x_A$  for antiproton production by polarized protons. The curve corresponds to a fit by eq. (6) with the parameters given in Table 5.

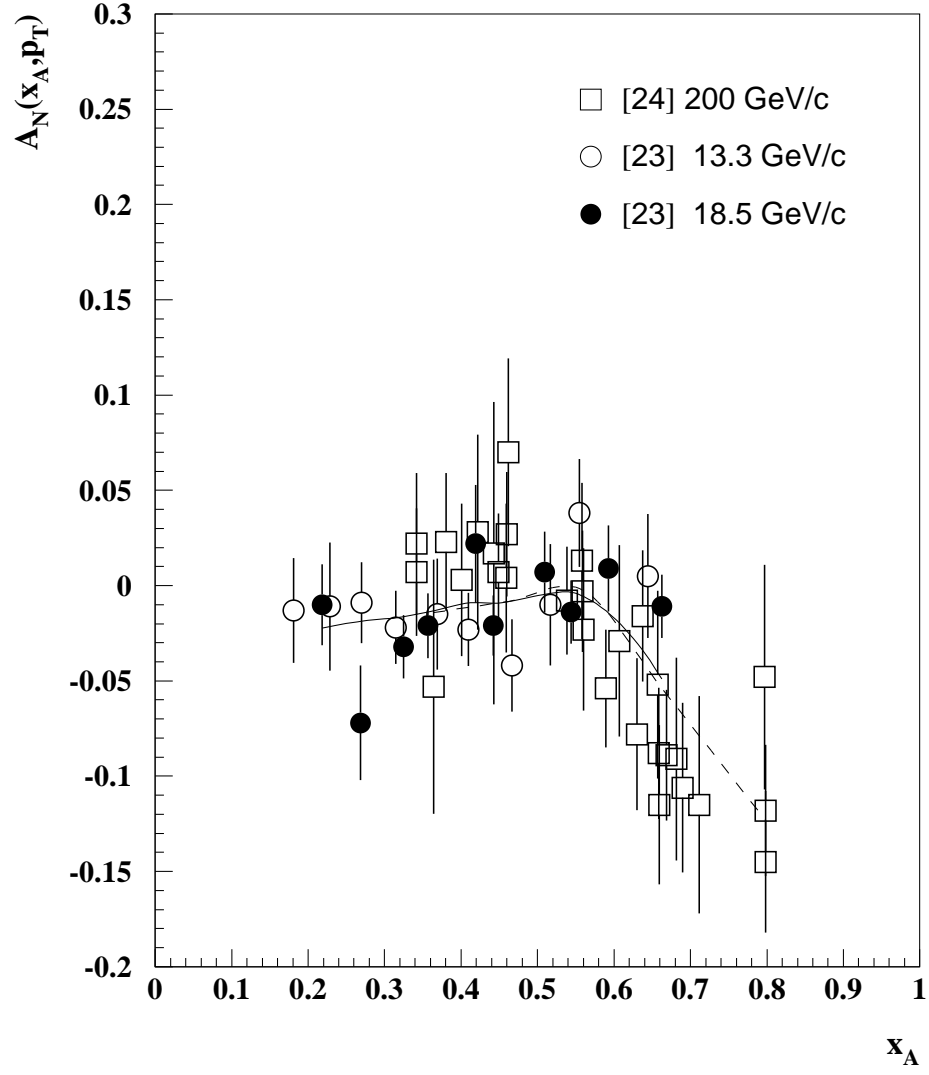


Figure 15:  $A_N$  vs  $x_A$  for the  $\Lambda$  production by polarized protons. The solid fitting curve corresponds to the 18.5 GeV/c data [23], and the dashed curve corresponds to the 200 GeV/c data [24].

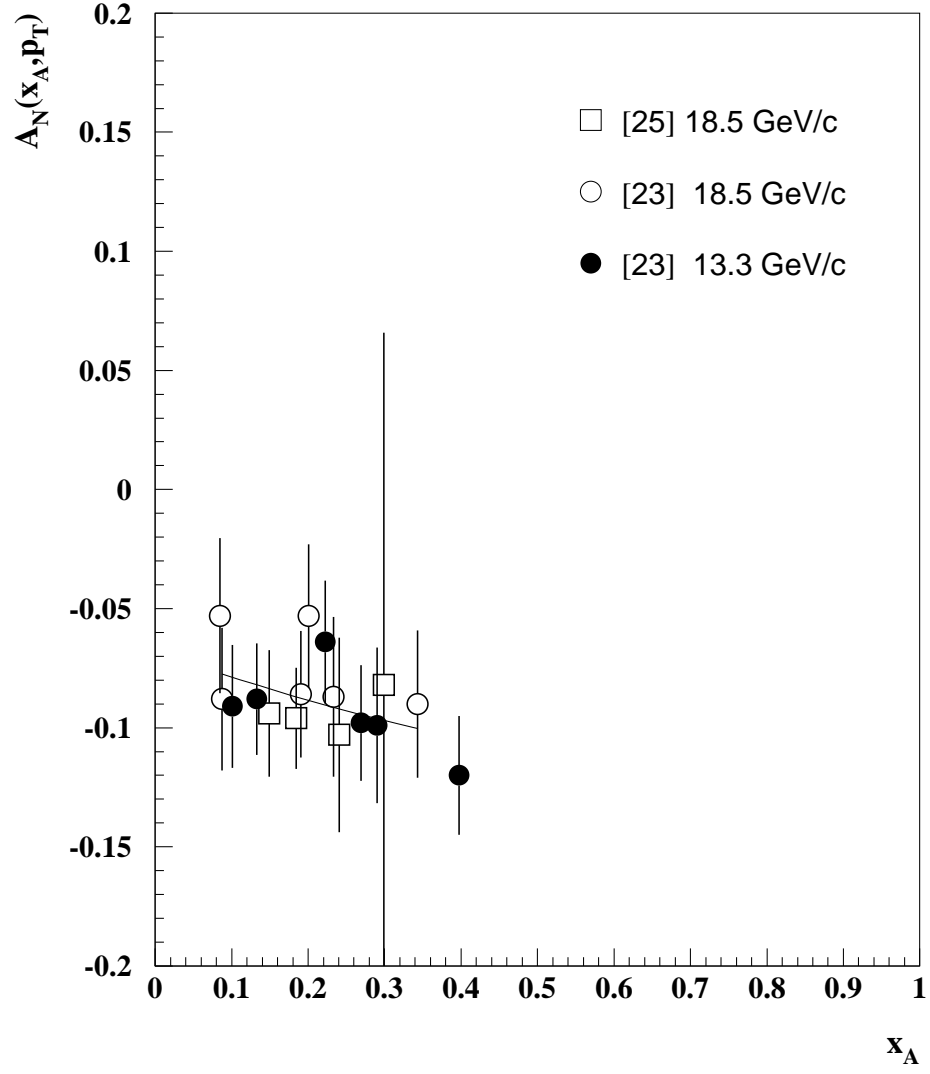


Figure 16:  $A_N$  vs  $x_A$  for the  $K_S^0$  production by polarized protons. The fitting curve corresponds to the 18.5 GeV/c data [23].

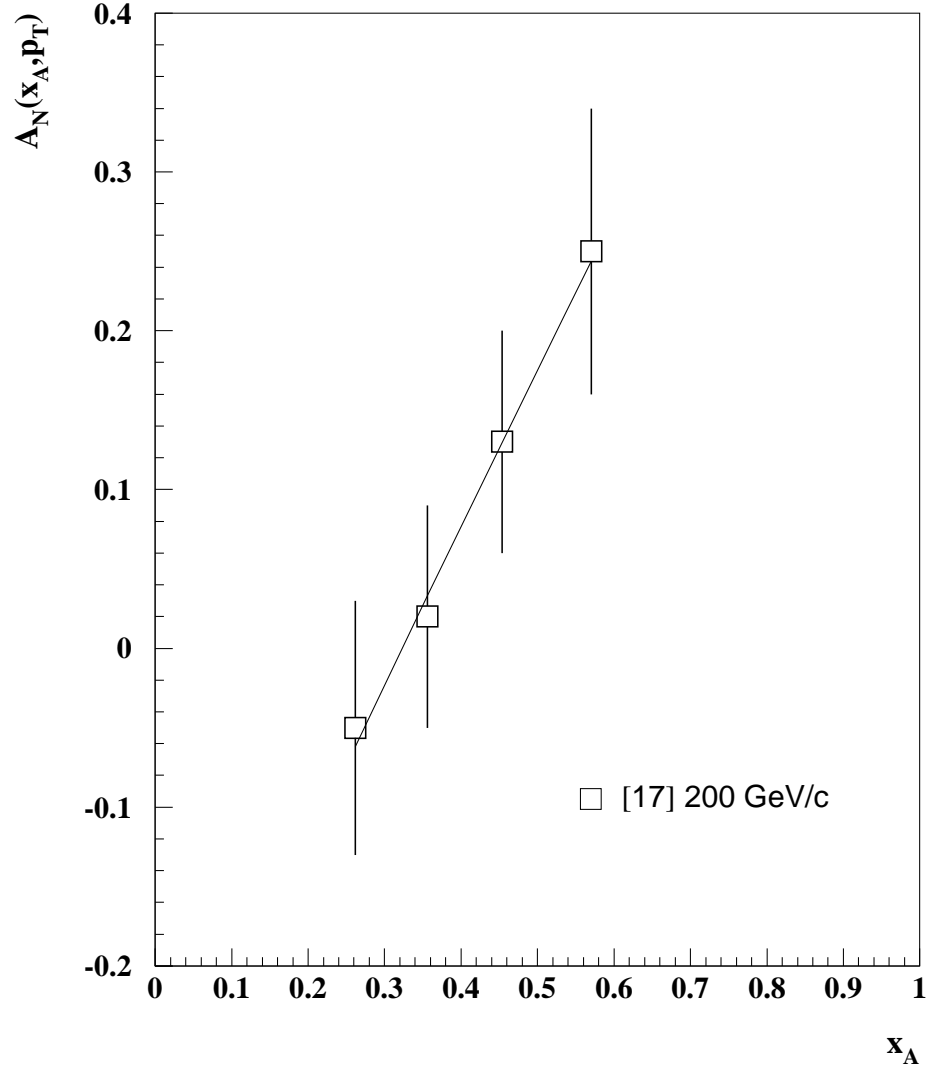


Figure 17:  $A_N$  vs  $x_A$  for the  $\eta$  production by polarized protons. The curve corresponds to a fit (6) with the parameters given in Table 7.

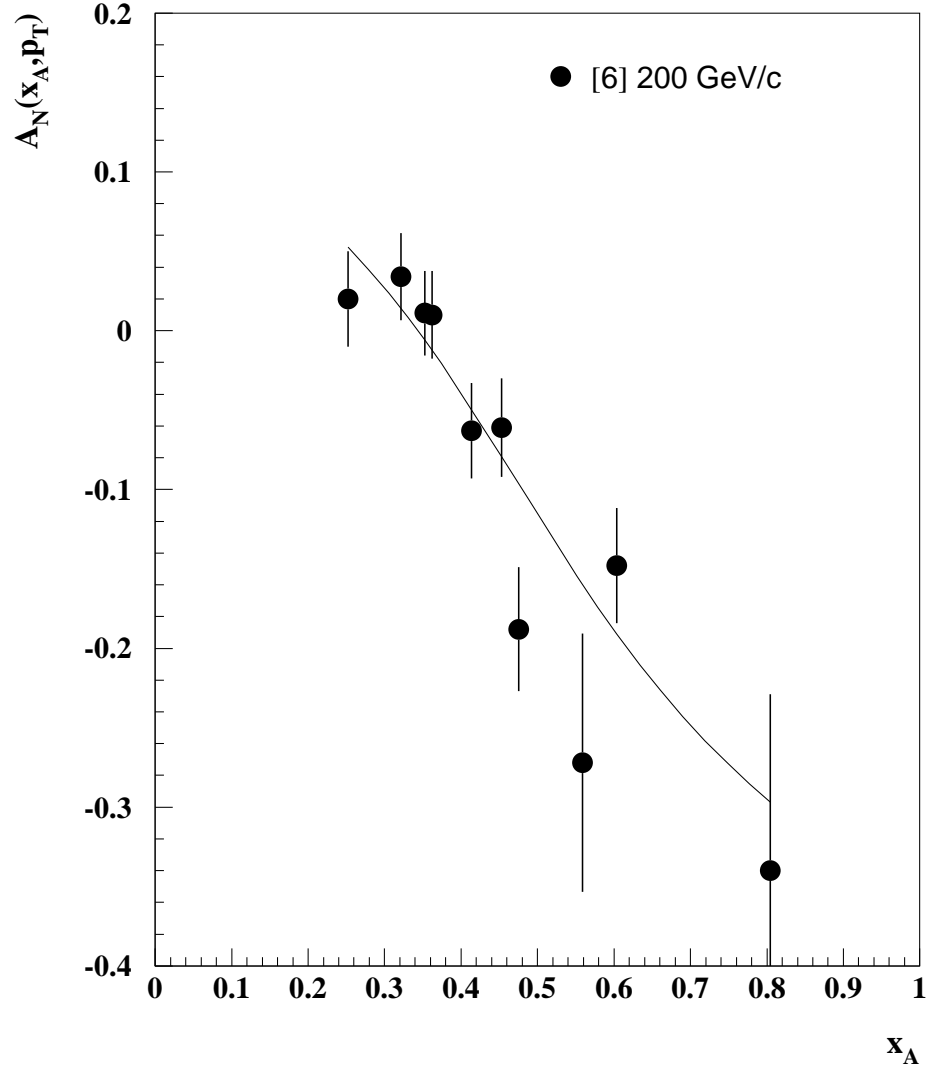


Figure 18:  $A_N$  vs  $x_A$  for the  $\pi^+$  production in  $\bar{p}p$ -collisions. The curve corresponds to a fit by eq. (6) with the parameters given in Table 9.

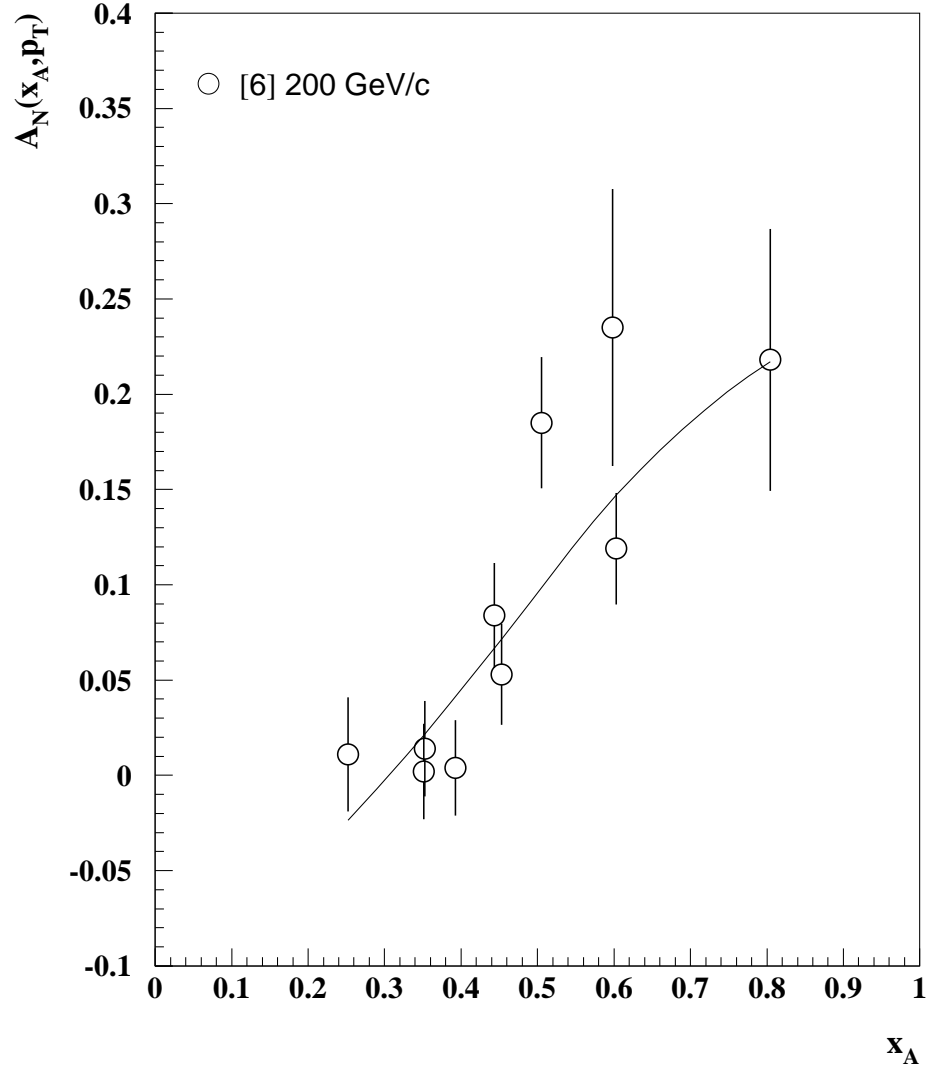


Figure 19:  $A_N$  vs  $x_A$  for the  $\pi^-$  production in  $\bar{p}p$ -collisions. The curve corresponds to a fit by eq. (6) with the parameters given in Table 9.

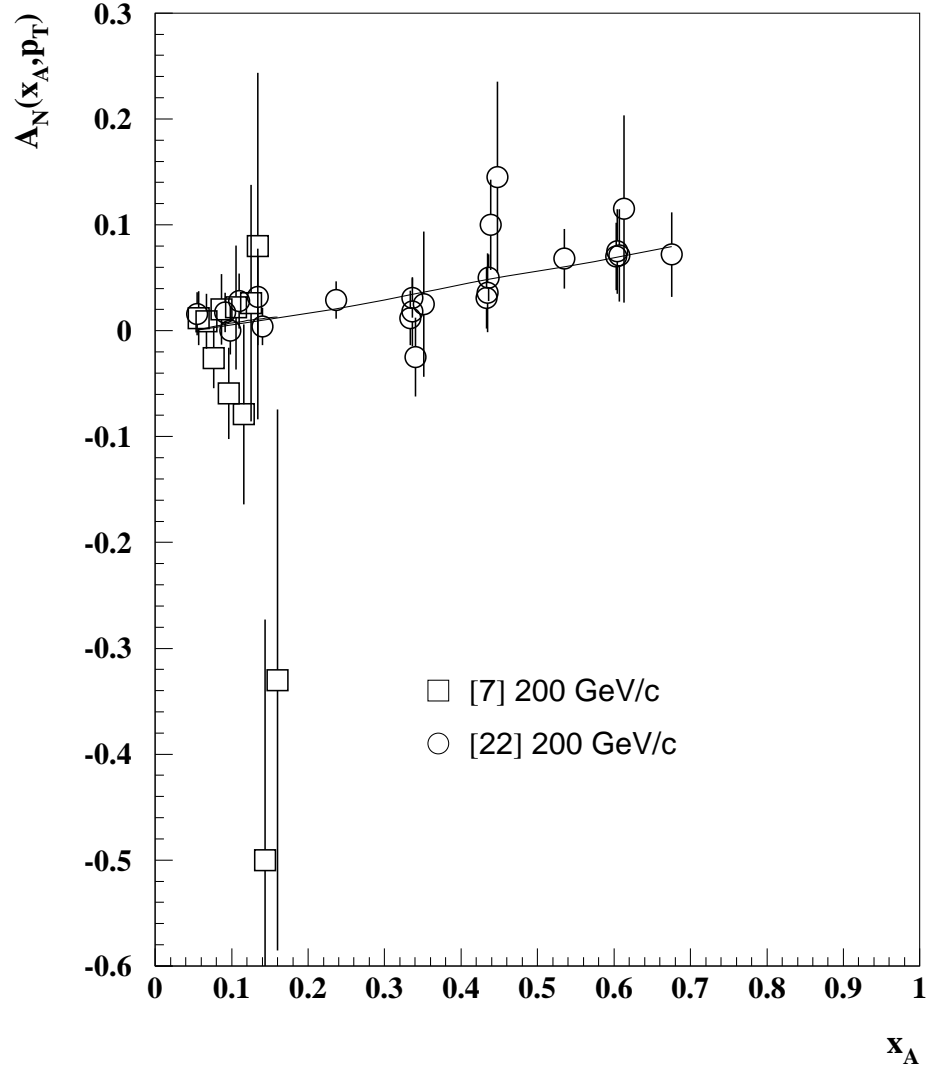


Figure 20:  $A_N$  vs  $x_A$  for the  $\pi^0$  production in  $\bar{p}^\uparrow p$ -collisions. The fitting curve corresponds to the 200 GeV/c data [22].

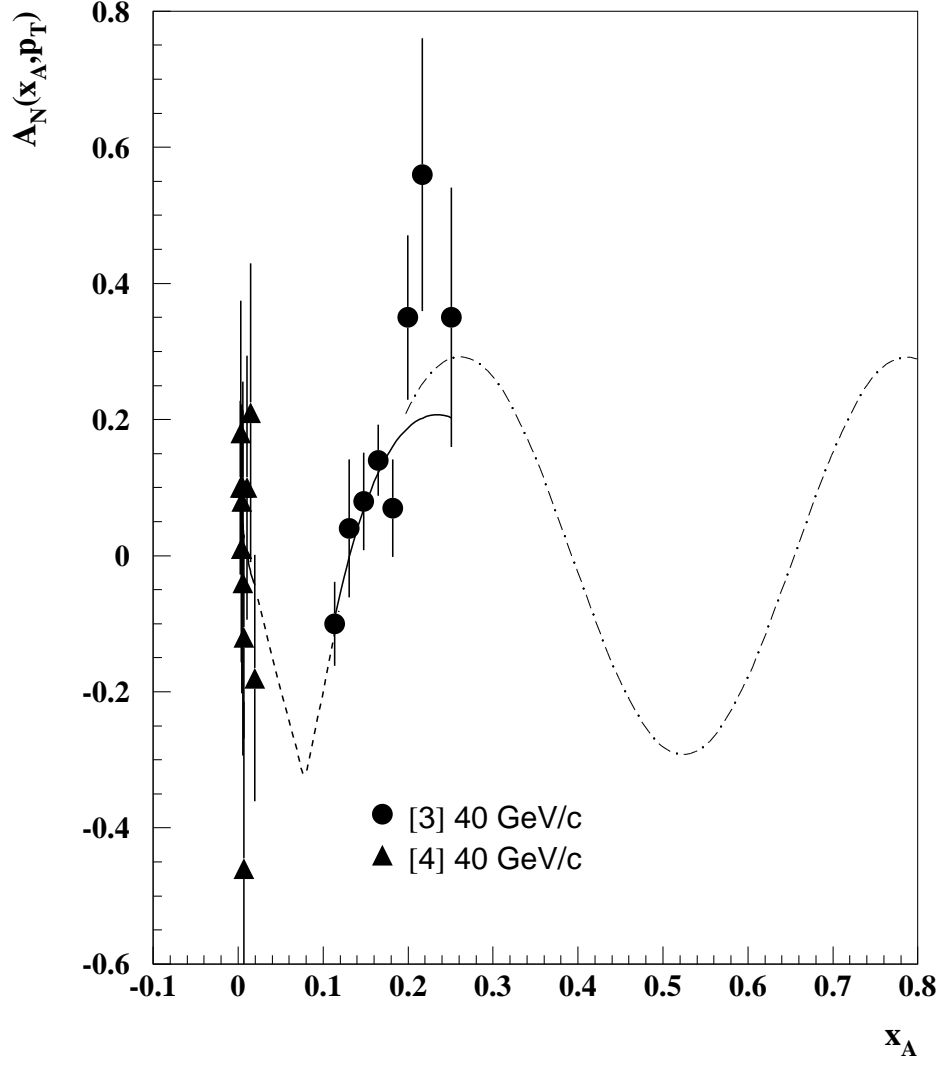


Figure 21:  $A_N$  vs  $x_A$  for the  $\pi^0$  production in  $\pi^- p^\uparrow$ -collisions. The solid curve corresponds to a fit by eq. (6) with the parameters given in Table 8. The dashed curve corresponds to an extrapolation of the fit (6) for the region  $p_T=1$  GeV/c and  $0.03 \leq x_A \leq 0.1$ . The dash-dot curve corresponds to an extrapolation of the fit (6) for the region  $p_T=2$  GeV/c and  $x_A \geq 0.3$ .

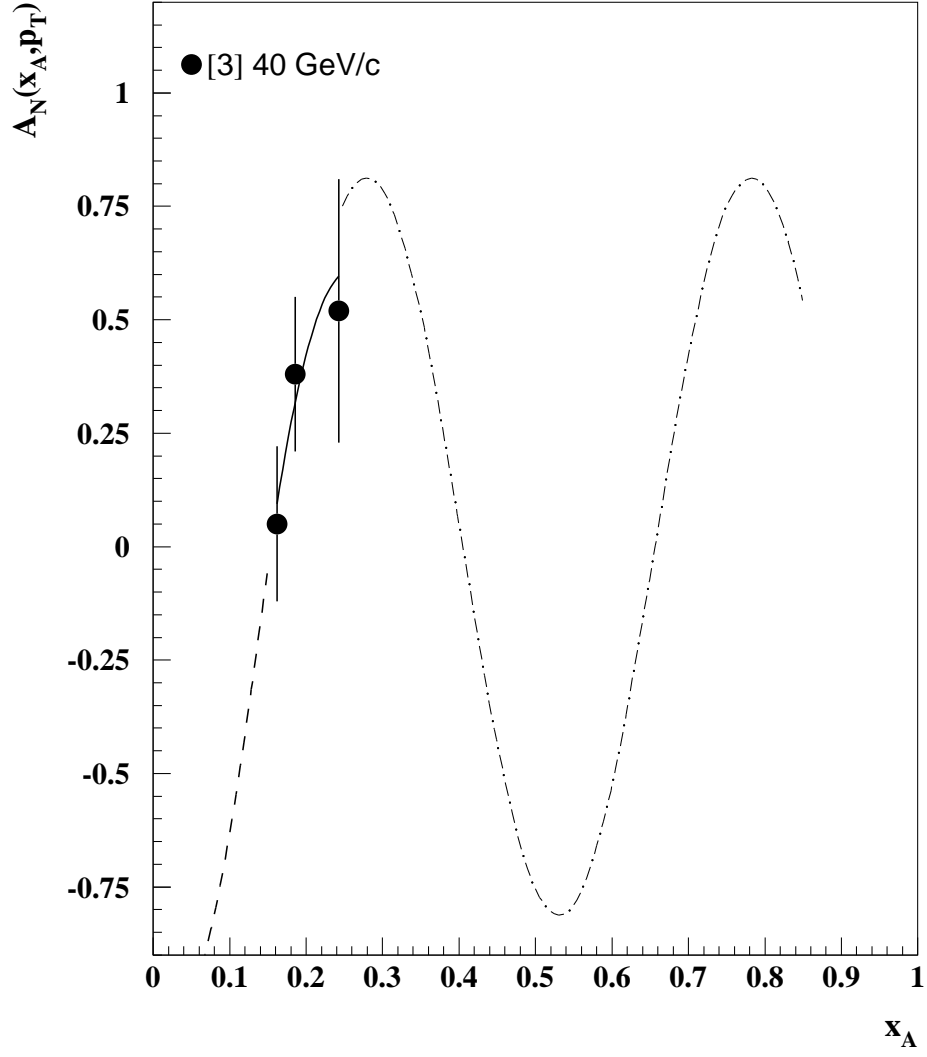


Figure 22:  $A_N$  vs  $x_A$  for the  $\eta$  production in  $\pi^- p^\dagger$ -collisions. The solid curve corresponds to a fit by eq. (6) with the parameters given in Table 8. The dashed curve corresponds to an extrapolation of the fit (6) for the region  $p_T=1 \text{ GeV}/c$  and  $x_A \leq 0.15$ . The dash-dot curve corresponds to an extrapolation of the fit (6) for the region  $p_T=2 \text{ GeV}/c$  and  $x_A \geq 0.3$ .

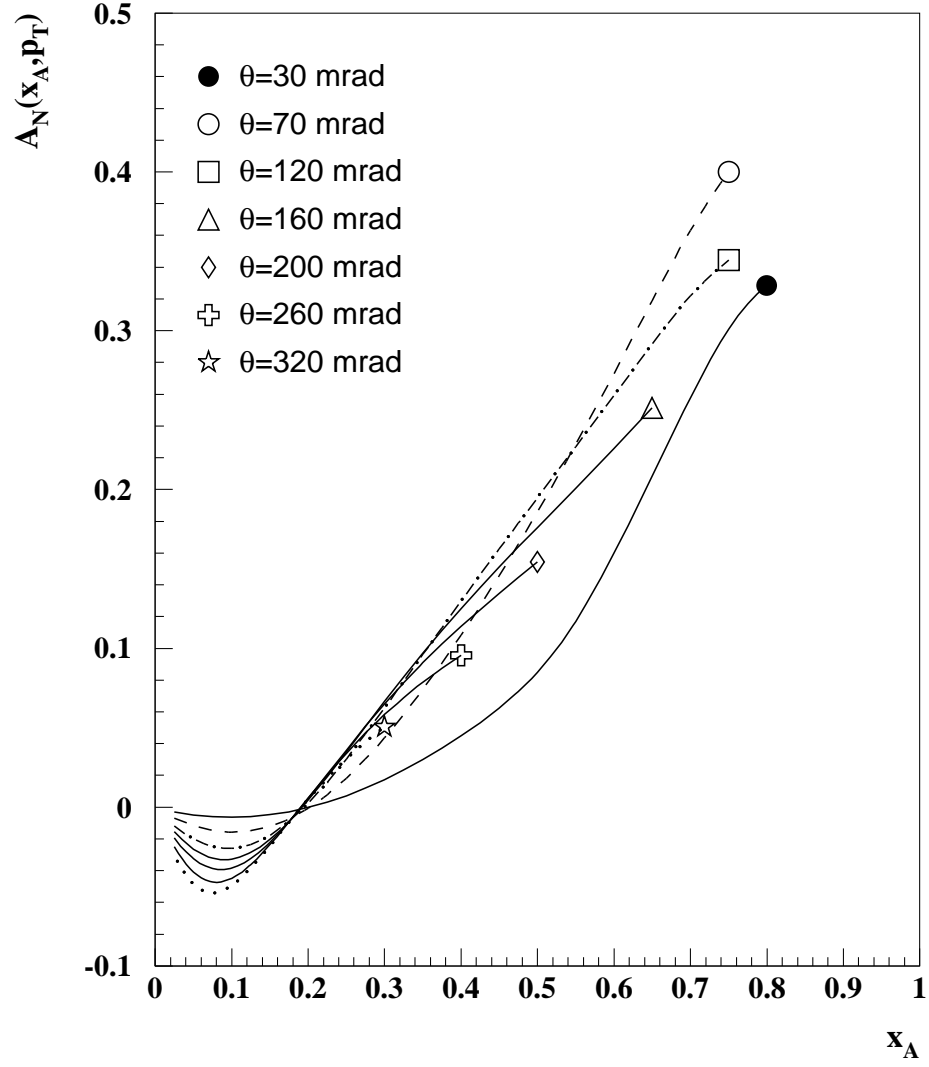


Figure 23: Predictions of the  $A_N$  vs  $x_A$  for the  $\pi^+$  production by polarized 40 GeV/c protons at the different laboratory angles.

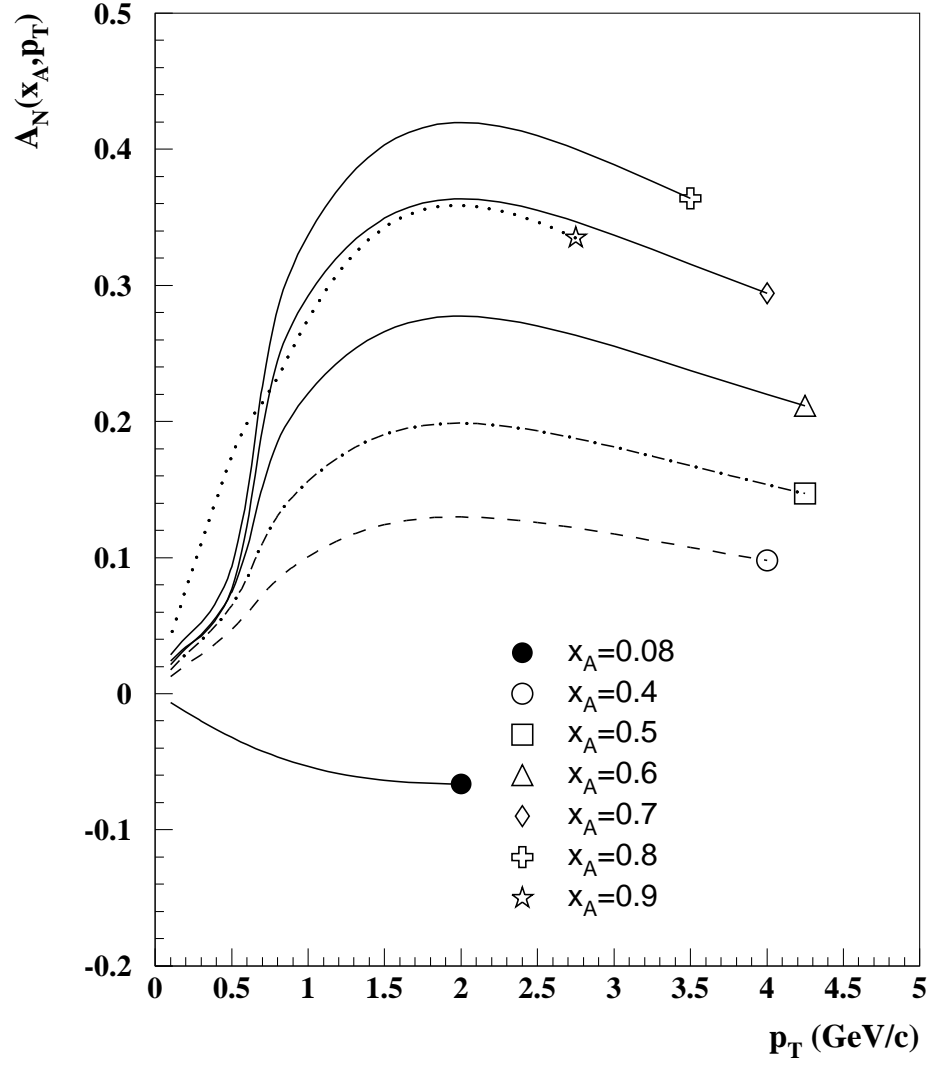


Figure 24: Predictions of the  $A_N$  vs  $p_T$  for the  $\pi^+$  production by polarized 40 GeV/c protons at the different  $x_A$  values.

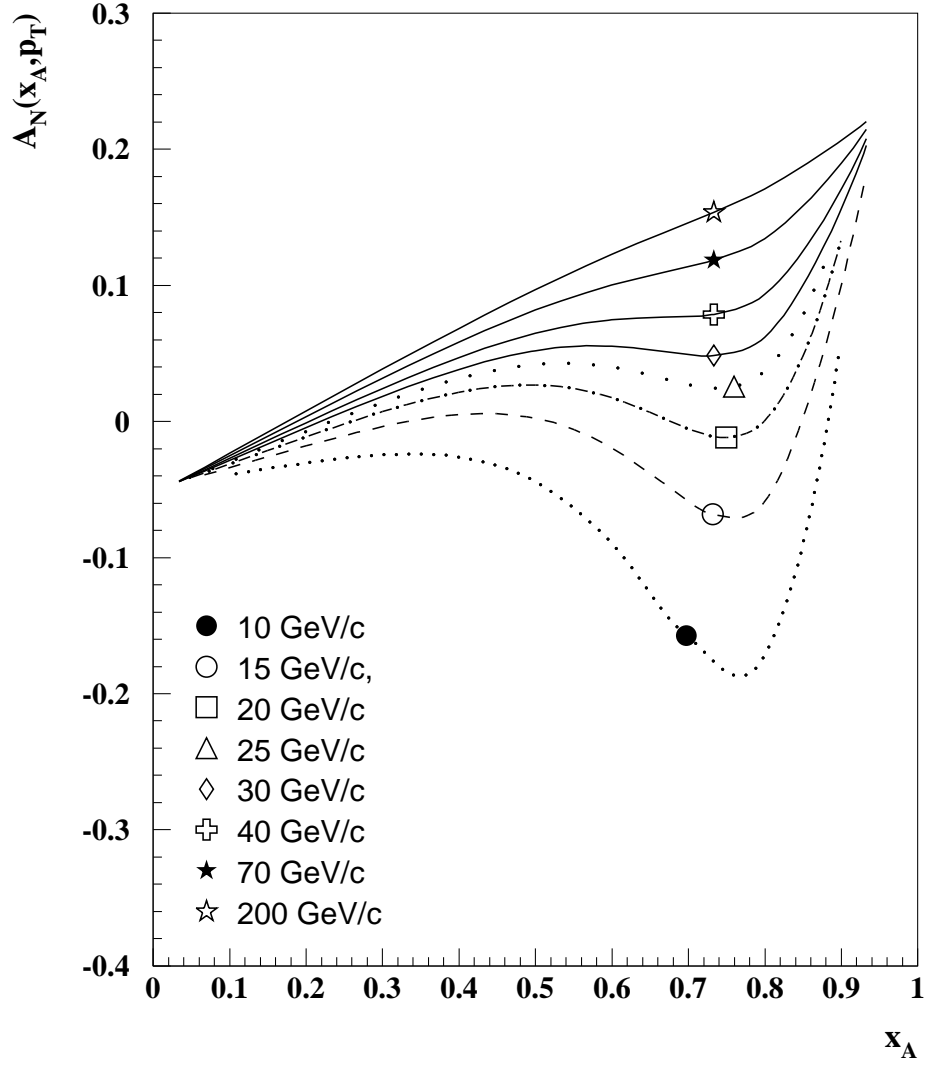


Figure 25: Predictions of the  $A_N$  vs  $x_A$  for the  $\pi^+$  production by polarized protons at the different beam energies and  $p_T = 0.5$  GeV/c.